2022

Effects of myosuppressin, a peptide neuromodulator, on membrane currents in the crustacean cardiac ganglion

Anthony Yanez
Bowdoin College

Effects of myosuppressin, a peptide neuromodulator, on membrane currents in the crustacean cardiac ganglion

An Honors Project for the Program of Neuroscience

By Anthony Yanez

Bowdoin College, 2022

Table of Contents

TABLE OF FIGURES

Acknowledgments

I would like to thank Patsy and Dan for all their help this year; their guidance made all the experiments performed in this study possible. A special thanks goes out to David Schulz, Joe Viteri, and Virginia Garcia at the University of Missouri, who hosted us and provided help with the RT-qPCR experiments. This research would not have been possible without funding from the Maine INBRE NIH grant #P20 GM 103423 from NIGMS, the Henry L. and Grace Doherty Charitable Foundation Coastal Studies Fellowship, and the Alan and Marsha Paller Neuroscience Fellowship.

Abstract

Central pattern generators are neural circuits that can independently produce rhythmic patterns of electrical activity without central or periphery inputs. They control rhythmic behaviors like breathing in humans and cardiac activity in crustaceans. Rhythmic behaviors must be flexible to respond appropriately to a changing environment; this flexibility is achieved through the action of neuromodulators. The cardiac ganglion of *Homarus americanus*, the American lobster, is a central pattern generator made up of four premotor neurons and five motor neurons. Membrane currents in each cell type, which can be targeted for modulation by various molecules, generate rhythmic bursts of action potentials. Myosuppressin, a FMRFamide-like peptide, is one such neuromodulator. The currents targeted for neuromodulation by myosuppressin are unknown. I investigated the molecular and physiological underpinnings of the modulatory effect of myosuppressin on motor neurons in the cardiac ganglion. First, using single cell RT-qPCR, I determined that across animals, motor neurons express myosuppressin receptor subtype II at equal levels relative to each other. Using sharp intracellular recordings, I showed that myosuppressin decreased burst frequency and the rate of depolarization during the inter-burst interval. I predicted that this effect resulted from the modulation of either A-type potassium current or calcium-dependent potassium current. Using two-electrode voltage clamp, I found that total outward current did not substantially change after treatment with myosuppressin. This result was surprising and provides grounds for explorations of subtle forms of neuromodulation in simple neural circuits.

Introduction

Central pattern generators, or CPGs, are neural circuits capable of independently producing rhythmic patterns of electrical activity in the absence of central or peripheral inputs. They are key to the control of rhythmic behaviors like undulatory swimming in lampreys, digestion in crustaceans, and breathing in humans (Marder and Bucher, 2001). It has been argued that neocortical circuits in mammals are analogous to CPGs (Yuste et al., 2005). Studies of CPG function have remarkably deepened our understanding of neural circuit function, neural cell types, and the biophysics underlying complex neural activity. Because they can produce fictive activity *in vitro*, CPGs continue to be of interest for revealing the principles that govern neural circuit function.

CPGs must be both robust and flexible to appropriately respond to changes in the environment. This flexibility is mediated by endogenous and exogenous modulatory molecules. Because CPG neurons often rely upon bursts of action potentials, it is often the case that neuromodulators which modify ion channel properties, do so by targeting channels that are responsible for generating bursts. Molecular, cellular, and computational approaches can be combined to study the process of neuromodulation in CPGs. CPGs must be robust and flexible to appropriately respond to changes in the environment; this flexibility is mediated by endogenous and exogenous modulatory molecules. Bursting is a complex process, and neuromodulatory signaling systems must overcome obstacles presented by variability in membrane current balance and synaptic strength in CPGs to consistently produce changes in output (Goaillard and Marder, 2021). This study aims to contribute more broadly to our understanding of how changes at the level of membrane currents alter patterned activity in neural circuits. The experiments reported here investigated the molecular and physiological mechanisms underlying neuromodulation by a

neuropeptide in a simple neural circuit. In the following passages, I will develop an understanding of how ion channel dynamics lead to bursting in CPGs, which is informed by computational and in-vivo experimentation.

Mechanisms of central pattern generation

To deepen our understanding of how CPGs are modulated, we must first develop a framework for how CPGs work generally. Central pattern generation in rhythmically active neural circuits is determined by the population of membrane currents and synaptic connectivity. For example, a tonically firing neuron may adopt a bursting pattern if its activity is driven by an intrinsically bursting neuron. Alternatively, two tonically firing neurons may adopt bursting activity if they inhibit each other and activate ionic membrane currents that cause rhythmic bursting. Membrane currents are carried by distinct ion channel proteins, each with unique gating variables dependent on time, voltage, and intracellular calcium concentrations (Marder and Bucher, 2007). Gating variables describe how channels activate and inactivate; the number of gates, their kinetics, and their dependencies determine ion channel function. Steady-state activation and inactivation functions describe ion channel activation and inactivation gates as sigmoid curves fitted by Boltzmann functions ranging from 0 to 1, with 0 representing no probability of channel opening and 1 representing 100% probability of channel opening (Clerx et al., 2019). Activation curves can be determined experimentally by fitting normalized current-voltage plots.

Theories of CPG function have been informed by both experimental and computational approaches. Theoretical studies of rhythmic neural circuits have revealed that many different combinations of the same molecular building blocks can underlie equivalent patterned activity (Goaillard and Marder, 2021). Thus, the balance of ion channels, rather than their absolute

expression levels and conductance values, determine neuronal activity. The same neuron type across animals occupies an area of conductance space where optimal output is possible (Goaillard and Marder, 2021). In both biological and computational models of the crustacean stomatogastric ganglion, vastly different combinations of membrane current conductance values and synaptic connectivity lead to identical output (Prinz et al., 2004; Schulz et al., 2006). Bursting mechanisms are not confined to a single set of parameters, as distinct ionic mechanisms of bursting can occur in the same cells (Harris-Warrick and Flamm, 1987). Models of single bursting neurons indicate that specific current types contribute to subsections of the burst waveform: the A-type potassium current (I_A) is active during the slow, rising driver potential, while the calcium-dependent potassium current (I_{KCa}) is most active at the end of the burst (Alonso and Marder, 2019). Other modeling work has shown that I_A and I_{KCa} are especially important for the generation and termination of slow oscillations in membrane potential that underlie the rhythmic nature of CPG activity (Franklin et al., 2010). The expression of Shal and I_H mRNA, which encode I_A and I_H ion channels, in pyloric neurons of the stomatogastric ganglion in crabs, which produces triphasic patterned output, are positively correlated, indicating that a balance of specific current subtypes preserves optimal electrical output (Schulz et al., 2006). I_A mRNA injection into crustacean neurons causes an increase in I_H, indicating that they are coregulated (MacLean et al., 2003). Maintaining these properties over time is not trivial and many of these processes show homeostatic regulation (Turrigiano and Nelson, 2004). By sensing their own activity, biological and model neurons can alter ion channel conductance values or chemical and electrical synapse strength to maintain a set point of electrical activity (Turrigiano and Nelson, 2004; O'Leary et al., 2013; Lane et al., 2016a). The balance of membrane currents differs between model bursting neurons with identical activity; perturbation thus presents a

unique challenge to cells maintaining consistent neural output. A decrease in I_A in two models, for example, can elicit different effects from different model bursting neurons (Alonso and Marder, 2019). Redundancy in neural circuit parameters provides a mechanism for robustness in electrical output. It also presents a problem for neuromodulatory systems; neural responses to modulation can be state-dependent, where change in output depends on the current landscape.

Lobster cardiac ganglion

The cardiac ganglion, or CG, is a simple CPG that controls cardiac activity in *Homarus americanus*, the American lobster, and other crustacean species. Its well-characterized anatomy and physiology make it a useful model for studying CPG function and modulation (Figure 1). It consists of 5 large motor neurons (large cells, or LCs) and 4 small pacemaker neurons (small cells, or SCs) (Cooke, 2002a). SCs produce sustained and frequent driver potentials that elicit bursts of action potentials; SCs also synapse with LCs, which cause rhythmic heart contractions. SCs and LCs are also strongly electrotonically coupled with a variety of innexin proteins; these coordinate activity between neurons in the CG and contribute to burst synchrony (Lane et al., 2016a). Burst duty cycle and burst frequency encode important information for muscle contraction, and the phase relationship between LC bursts and SC bursts varies from animal to animal (Williams et al., 2013a, 2013b). The CG and heart receive descending input from thoracic ganglia (Cooke, 2002a). The pericardial organ, an important source of neurohormones, is located ventral to the heart and releases hormone molecules into the hemolymph to diffuse into the cardiac system (Cooke, 2002a). Given its simple anatomy and large, accessible motor neurons, the CG has proven to be a valuable model neural circuit for the study of basic principles of central pattern generation.

Understanding the specific mechanisms of rhythmic burst generation in the lobster CG greatly informs studies of neuromodulation using this system. The membrane currents underlying driver potentials in LCs of *H. americanus* are well-understood and include sustained calcium (I_{CaS}), transient calcium (I_{CaT}), calcium-activated potassium (I_{KCa}), and A-type potassium (I_A) currents (Figure 2) (Tazaki and Cooke, 1986). Driver potentials are localized to the soma and initial axon segment of LCs in the crustacean CG (Cooke, 2002b). The driver potential is an active process; once an LC is stimulated to threshold, the complete driver potential initiates. Because LCs are electrotonically coupled, initiation of a driver potential in one LC causes driver potentials in all LCs (Cooke, 2002b). The dynamics of channel function depend on membrane potential and time, and dictate the rising, sustained, and falling phases of the LC driver potential and burst. The depolarization, or rising, phase of the driver potential in *H. americanus* is mediated by voltage-gated calcium channels with fast and slow kinetics, declining with time constants of 40 ms and 180 ms, respectively (Tazaki and Cooke, 1990). Maximum calcium current in voltage clamp is achieved with a holding step of -60 mV (Cooke, 2002b). Accumulation of intracellular calcium during the driver potential causes I_{KCa} to activate and quickly hyperpolarize membrane potential and also contributes to the deactivation of calcium channels and termination of the LC burst (Cooke, 2002b). Slowly-inactivating potassium current inactivates rapidly after repolarization and outward I_{KCa} diminishes as intracellular calcium is sequestered (Cooke, 2002b). Because it may take time for the intracellular calcium concentration to drop, I_{KCa} can also contribute to the frequency of driver potentials. This calcium channel inactivation leads to a burst refractory period, whereby the next driver potential cannot occur until calcium is sequestered and calcium channels are deinactivated. Because previous activity increases the amount of intracellular calcium, driver potential frequency is closely tied to driver

potential duration. A slow potassium current counteracts the depolarizing effects of inward calcium currents in *H. americanus* (Cooke, 2002b). Inward sodium currents, like persistent sodium (I_{NaP}), may also be involved in the depolarization phase of the pacemaker potential; evidence for a TTX-sensitive I_{NaP}-like current is present in *Cancer borealis* CG LCs (Ransdell et al., 2013). The burst contains a fast-decaying and slow-decaying phase, likely due to different hyperpolarizing currents (Cooke, 2002a). In CG LCs, I_A peaks at about 5 ms and decays with a time constant of about 200 ms (Tazaki and Cooke, 1986). Because I_A is voltage dependent and active starting at -40 mV, it contributes to driver potential frequency by transiently dampening pacemaker depolarization. LCs display varying driver potential responses to TEA treatment, with more anterior cells showing far more driver potential depolarization (Berlind, 1993). This indicates that I_{Ca} or I_{KCa} may differ along the anterior-posterior axis. However, ion channel and innexin mRNA expression levels do not differ between LCs in the CG, indicating that they are largely identical (Schulz, personal communication).

Neuromodulation

CPG flexibility is mediated by neuromodulation. Modulators act on receptors at the surface of cells to elicit a vast array of effects including, but not limited to, the opening of ion channels (Marder and Bucher, 2007). Changes in ion channel kinetics can drastically alter the intracellular environment and ultimately, network activity; modeling studies of the pyloric network in crab STG reveal that calcium channel kinetics can cause enhancement of the inhibitory synapse between the lateral pyloric and pyloric dilator neurons (Oh et al., 2012). Neuromodulators can have various underlying mechanisms of action; a single neuromodulator can target a subset of cells in a neural circuit (Swensen and Marder, 2000; Marder and Bucher, 2007). Within those cells, a single neuromodulator can alter properties of different ion channels.

Alternatively, multiple different modulators could converge on the same ionic current in the same cell (Marder et al., 2014). For example, proctolin, a neuropeptide modulator found in crabs and lobsters, activates a voltage dependent inward current (I_{MI}) (Golowasch and Marder, 1992). However, a variety of other modulators found in these animals operate ion channels with identical current-voltage relationships (Swensen and Marder, 2001).

Ion channel kinetics are an important class of channel properties and are also targets of modulation; the speed with which ion channels change conformation to pass current dictates the time during which that current is active. At subthreshold membrane potential values, transient currents like I_A are important for controlling neuronal excitability in single cells and neural circuits (Golowasch et al., 1992). I_A, which has voltage-dependent activation and inactivation gates, is active during a subthreshold window near -40 mV (this value can vary from system to system and depends strongly on protein structure; Connor and Stevens, 1971a). Thus, I_A is well-positioned to control neuronal excitability and rhythmic activity (Connor and Stevens, 1971b). Indeed, there are many examples of I_A doing so in various contexts. Rhythmic activity in hippocampal cells is mediated by I_A (Bourdeau et al., 2007). Calmodulin inhibitors slow the inactivation kinetics of I_A in rat smooth muscle cells (Kryshtal' et al., 2007). Studying ion channel kinetics in the CG will thus inform how work in other systems.

Activation and inactivation kinetics and voltage-dependence are important targets of modulatory compounds in many cells with excitable membranes. The voltage-dependence of I_A can also be modulated to influence neuronal output. I_A is sensitive to intracellular calcium (Amendola et al., 2012). In rats, a group of calcium-sensing proteins increase conductance magnitude, slow inactivation, and hyperpolarize I_A voltage-dependence (An et al., 2000). Whether these I_A-modulating calcium-sensing proteins are expressed in crustacean neurons is

unknown. I_A delay kinetics in cultured rat hippocampal neurons are slowed by a urea compound (Witzel et al., 2012). In the crustacean STG, dopamine modulates pyloric rhythm activity by depolarizing I_A voltage-dependence and decreasing maximal conductance (Harris-Warrick et al., 1995). I_A and I_{KCa} also contribute to robustness in neural circuits; I_A current density in inferior cardiac neurons in the crab stomatogastric nervous system is regulated in a calcium-dependent manner to relieve the effects of prolonged depolarization (Golowasch et al., 1999). It is likely that modulators that target neurons in the CG elicit similar changes in ion channel kinetics and gating parameters to alter overall CG output.

Neuropeptides are an important class of signaling molecules in the nervous system. They are abundant across species, from crustaceans to humans. Peptidergic signaling is ancient and is present even in placozoans (Varoqueaux et al., 2018). Neuropeptide cotransmission occurs alongside neurotransmitters like glutamate or GABA (Nusbaum et al., 2017). Neuropeptides are stored in dense core vesicles with a release probability distinct from vesicular neurotransmitters (Nusbaum et al., 2017). Neuropeptide biosynthesis involves translational and post-translational processing, which leads to various peptide isoforms (Nusbaum and Blitz, 2012). Such processing is key for maintaining bioactivity; in mice, eliminating neuropeptide amidation in forebrain neurons decreases anxiety behavior and improves thermoregulation (Powers et al., 2019). In the mammalian brain, dynorphin and enkephalin are endogenous neuropeptides that act on κ- and μ-opioid receptors to modulate signaling in pain and reward circuitry. Peptidergic signaling has recently gained attention as an important system for homeostasis and information processing in mammals. In invertebrates, neuropeptides have been found to profoundly alter circuit output, especially in pattern-generating microcircuits (Nusbaum and Blitz, 2012). Peptidergic signaling also plays an important role in many lobster neural circuits, and a plethora of neuropeptides have

been characterized using mass spectrometry and bioinformatic techniques (Christie et al., 2015). There are numerous examples of neuropeptide modulation in crustacean neural circuits at a variety of targets. Red pigment concentrating hormone elicits an increase in synaptic strength that merges the cardiac sac and gastric mill rhythms in the STG into one rhythm with elements of both (Dickinson et al., 1990). Co-application of two neuropeptides, RPCH and CabTRP, onto the stomatogastric ganglion elicits effects distinct from each peptide separately (Nusbaum et al., 2017). Thus, crustacean neural circuits are valuable models that can inform our understanding of peptidergic across species and contexts, including modulatory circuits implicated in human disease.

Myosuppressin

Myosuppressin, an FMRFamide-like peptide, is a well-characterized modulator named after its inhibitory effect on insect muscle tissue (Nässel, 2002). Crustacean myosuppressin, pQDLDHVFLRFamide, was first identified by mass-spectrometry in lobster commissural ganglia; it contains a pyroglutamic acid at its C-terminus and an amide group on its N-terminus (Stemmler et al., 2007). Crustacean myosuppressin decreases heart contraction frequency but increases heart contraction amplitude in the lobster in a dose-dependent manner. Additionally, myosuppressin decreases isolated CG burst frequency, but increases burst duration in a dose-dependent manner (Stevens et al., 2009). Post-translational processing is important for myosuppressin bioactivity; QDLDHVFLRFamide, but not pQDLDHVFLRF, decreases CG burst frequency and increases burst duration similar to pQDLDHVFLRFamide (Oleisky et al., 2022). This is consistent with docking studies of the RFamide family of peptides, which show that the C-terminal FMRFamide interacts strongly with FMRFamide receptors, while the N-terminus unique to each neuropeptide confers specificity (Maynard et al., 2013). Immunohistochemistry

on fixed CG reveals myosuppression immunoreactivity throughout the CG, indicating that both the SCs and LCs receive modulatory myosuppressin input (Stevens et al., 2009). Prepromyosuppressin mRNA transcripts are also found in CG tissue, suggesting it is synthesized and released locally (Oleisky et al., 2020). Myosuppressin acts on cellular subtypes in the CG differentially; low concentrations decrease burst frequency in LCs and increase duty cycle in SCs (Oleisky et al., 2020). Intracellular recordings in LCs show that myosuppressin causes a drastic hyperpolarization of resting membrane potential in addition to decreasing burst frequency (Stevens et al., 2009).

Myosuppressin receptor structure and ligand-binding in insects is well-characterized. Multiple myosuppressin receptors have been discovered and sequenced in *Drosophila melanogaster* (Nichols, 1992; Egerod et al., 2003). *Drosophila* myosuppressin receptors are members of the rhodopsin-like family, a G protein-coupled receptor (GPCR) family that functions with an ionic lock mechanism of activation (Bass et al., 2014; Leander et al., 2015). Docking studies show that subtle differences in the *Drosophila* myosuppressin receptor binding pocket influence peptide conformation and specify which ligands can bind (Bass et al., 2014). *Drosophila* myosuppressin activates two different putative myosuppressin receptors *in vitro* to decrease GTPγS binding, with no changes in intracellular calcium concentration or cAMP; interestingly, activating the same receptor with forskolin induces a decrease in cAMP, suggesting that myosuppressin receptors couple with G_i proteins (Johnson et al., 2003). A homology search of the lobster transcriptome from brain and eyestalk ganglia reveals five putative myosuppressin receptors: myosuppressin receptors I – V. Additionally, RT-PCR shows that CG SCs and LCs preferentially express different myosuppressin receptor subtypes; SCs express more myosuppressin receptor IV, and LCs express more myosuppressin receptor II and III (Oleisky et

al., 2020). Unfortunately, this analysis informs us about neither the quantitative relationships among myosuppressin receptor subtype expression, nor the cellular distribution of myosuppressin receptors across the cells of the CG. This information would be incredibly useful for elucidating the mechanism of myosuppressin modulation in the CG.

Research question

The exact cellular and subcellular targets of myosuppressin are unknown. The bidirectional effects of myosuppressin on cardiac activity and CG bursting are especially interesting as there seem to be multiple underlying mechanisms. The decrease in resting membrane potential and burst frequency in response to myosuppressin may be explained by an enhancement of the outward current I_{KCa}, which is responsible for terminating the LC burst. Alternatively, enhancing the window current of I_A could inhibit the driver potential and slow bursting. I predict that myosuppressin enhances I_A and/or I_{KCa} to mediate its modulatory effect. To investigate this question, I used two-electrode voltage clamp and sharp intracellular recording methods on LCs in the lobster CG. I also used single cell RT-qPCR to investigate the expression pattern of myosuppressin receptor subtypes in individual motor neurons to further elucidate the modulatory targets of myosuppressin.

Methods

Animals

Adult *H. americanus* were obtained from local seafood markets (Brunswick, ME, USA). Experimental animals were approximately balanced in sex and varied in molt cycle stage. Animals were kept in tanks with seawater at 10℃ to 12℃ on a 12hr:12hr light-dark cycle and fed a diet of chopped fish and squid. Lobsters were anesthetized in ice for 30 minutes before dissection. CG were obtained by first removing a rectangular section of the dorsal carapace containing the heart, then cutting the cardiac musculature, ventral-side up, along the anterior-

posterior axis to reveal the CG. The two anterolateral branches were obtained, along with the main trunk. A section of posterior artery was kept to protect the SCs of the CG. Landmarks on the anterolateral branch were used to ensure the CG was pinned out ventral-side up. CG were pinned to a clear, Sylgard-coated petri dish. All dissections were performed in chilled physiological saline (479.12 mM NaCl, 12.74 mM KCl, 13.67 mM CaCl2, 20.00 mM MgSO4, 3.91 mM Na2SO4, 11.45 mM Trizma base, and 4.82 mM maleic acid; pH 7.44-7.46).

Tissue collection

Individual motor neurons were collected for single cell RT-qPCR at the University of Missouri in Columbia, MO. *H. americanus* (n=8) were shipped from Halifax, Nova Scotia and kept in tanks with seawater at 10 to 12℃ on a night-day cycle. CG were dissected as described above. A tissue landmark (usually a specific nerve process on the anterolateral nerve) was used to distinguish between cells 1 and 2 in each dissection. For each CG, every large cell was desheathed to expose the soma. Then, a 2 cm diameter Vaseline well surrounding the entire CG was made, filled with collagenase/dispase (Roche, catalog number 10269638001; 1 mg/mL in lobster saline) and left to digest connective tissue for 20 minutes. The well was then washed with three volumes of cold saline. Ethylene glycol (70% in lobster saline) was incrementally added to the well and the saline outside the well was replaced with distilled water. The dish was frozen at -20℃ for 45 minutes. After the distilled water completely froze, individual cells were plucked using sterile forceps, placed in 400 µL lysis buffer (Zymo Research, Irvine, CA, USA), and stored at -80℃.

RNA extraction

Collection of single cells, extraction of mRNA, cDNA synthesis, and qPCR were performed as reported previously (Santin and Schulz, 2019). For mRNA extraction, the *Quick*-

RNA Microprep Kit (Zymo Research, Irvine, CA, USA) was used according to manufacturer's instructions. Briefly, one volume of ethanol (100%) was added to each sample tube, transferred to a Zymo-Spin IC Column in a Collection Tube, and centrifuged for 30 seconds at 17,000×g. This was followed by one centrifugation step (17,000×g, 30 seconds) of RNA Prep Buffer (Zymo Research, 400 µL) and two centrifugation steps (17,000×g, 30 seconds each) of RNA Wash Buffer (Zymo Research, 700 µL and 400 µL). Then, each spin column was centrifuged with molecular water for 2 minutes to elute mRNA, and qScript cDNA SuperMix (QuantaBio, Beverly, MA) was added for a final volume of 20 µL for each sample.

cDNA synthesis and qPCR

To quantitatively measure the expression levels of mRNA transcripts from single cells using qPCR, cDNA copies of mRNA transcripts in each sample must be created. cDNA synthesis was performed using random hexamer and oligo-(dT) primers with qScript cDNA Supermix (QuantaBio, Beverly, MA, USA) according to manufacturer's instructions. Briefly, each sample was incubated at room temperature (five minutes), 42℃ (30 minutes), and finally 85℃ (five minutes) (Santin and Schulz, 2019). No preamplification step was performed. Primers against 18S rRNA were first used to assess cDNA quality (forward, 5'-AGGTTATGCGCCTACAATGG-3'; reverse, 5'-GCTGCCTTCCTTAGATGTGG-3'). Primers against MSRI (forward, 5'-AGCCGACCGGGTTACAAAAA-3'; reverse, 5'-CTCGGAGCCTAGAATGACCG-3') and MSRII (forward, 5'-CTGATGATCTGCCTGGTGGG-3'; reverse, 5'-GCAAGACCGGTGAGTATGGT-3') were used in separate reactions with input from the same cDNA samples. For 18S rRNA, qPCR was performed using 2x SsoAdvanced Universal Inhibitor-Tolerant SYBR Green Supermix (BioRad Laboratories, Hercules, CA, USA), molecular grade water, forward and reverse primers (10-fold

dilution of stock), and cDNA (0.5 µL) for a total reaction volume of 10 µL per well. For MSRI and MSRII, cDNA samples were diluted to 50 µL. Then, a qPCR reaction with 2x SsoAdvanced Universal Inhibitor-Tolerant SYBR Green Supermix (BioRad Laboratories, Hercules, CA, USA), MSR forward and reverse primers (10-fold dilution of stock), and cDNA (8 µL) for a total reaction volume of 10 µL per well was run using a BioRad CFX Connect Real-Time PCR Detection System with the following three-step cycle: 95℃ for 20 seconds, 58℃ for 20 seconds, and 72℃ for 20 seconds. A total of 40 cycles were performed, with fluorescence data acquired at 72℃ in each cycle. All qPCR reactions were performed in triplicate.

Electrophysiology

Temperature was maintained between 10℃ and 13℃ using an in-line Peltier temperature regulator (CL-100 bipolar temperature controller and SC-20 solution heater/cooler; Warner Instruments, Hamden, CT) with a temperature probe (Warner Instruments, Hamden, CT). Physiological saline was superfused at a flow rate of 5 ml/minute across the ganglion using a Rabbit peristaltic pump (Gilson, Middleton, WI).

Extracellular recordings were used to ensure the health of the CG. A Vaseline well was made around the CG trunk. Stainless-steel pin electrodes were used to monitor electrical activity. One pin was placed in the well and another was placed in the bath. Electrical output was recorded using a 1700 A-M Systems differential AC amplifier (Sequim, WA).

For intracellular recordings, a portion of the anterolateral branch of the CG was desheathed to expose the soma of either cell 1 or cell 2 (n=6). Glass electrodes (R = 13–20 MΩ) filled with squid cytoplasmic fill (20 mM NaCl, 15 mM Na_2SO_4, 10 mM Hepes, 400 mM potassium gluconate, 10 mM $MgCl_2$) in electrode holders containing silver wires were used to pierce the soma (Hooper et al., 2015). Silver electrodes and a silver ground wire were immersed

in bleach for approximately 15 minutes before each experiment to chloride the electrodes for stable recordings of electrical potential. The membrane potential was monitored using an AxoClamp 2B (Axon Instruments) and filtered using a Model 410 Brownlee Precision Instrumentation amplifier (Brownlee Instruments, San Jose, CA). For each experiment, baseline was recorded for 10 minutes. To determine if myosuppressin caused changes in resting membrane potential, cells bathed in TTX (10^{-7} M) were superfused with pQDLDHVFLRFamide, crustacean myosuppressin (10^{-6} M). Input resistance was measured in each cell by injecting 1 nA of current and measuring the change in membrane potential. All electrophysiological data were recorded to a PC and analog signal were digitized using a CED Micro 1401 USB interface and the data acquisition software Spike2.0 v9.01 (Cambridge Electronic Design, Cambridge, UK) at a sampling rate of 10 kHz.

Two-electrode voltage clamp (TEVC) was used to investigate modulation of specific ionic currents (Figure 3). Cardiac ganglia were removed from heart tissue and pinned to a Sylgard dish. The somata of cells one, two, or three (n=3) were exposed and the membranes pierced with two glass electrodes (R = 13 to 20 MΩ). Neurons with input resistances greater than 2 MΩ were used for TEVC experiments under TTX (10^{-7} M) and myosuppressin (10^{-6} M; Genscript, Piscataway, NJ). For each experiment, baseline was recorded for 10 minutes. Then, myosuppressin was superfused for 10 minutes. Finally, saline was superfused for 40 minutes to wash out the effects of myosuppressin. To test for changes in outward current, cells were held at -90 mV for 1 second followed by 500 millisecond steps increasing to 0 mV in increments of +10 mV (Figure 4). Holding the membrane potential at -90 mV for 1 sec deinactivates A-type potassium current, allowing for measurement of maximal outward current. After it was

discovered that A-type potassium current did not fully decay within 500 ms at high voltage steps, a 2 sec voltage command step was used.

Data analysis

Intracellular recordings were analyzed manually using cursors and cursor regions to measure the afterhyperpolarization and inter-burst interval slope in Spike2.0. Voltage clamp currents were measured at their peak. Electrophysiological data was organized in Microsoft Excel. RT-qPCR data were exported into, and processed in, Microsoft Excel. Two processing schemes were used; first, average quantification cycle (C_q) values for each target gene (18S, MSRI, MSRII) were used to compare between LCs 1–5. As an alternative analysis, the $2^{-\Delta\Delta Cq}$ was performed, using 18S as a reference gene and LC1 as an arbitrary control condition (Livak and Schmittgen, 2001). Processed data were plotted in Prism 9.0.4 (Graphpad Software, Inc.). Prism was used to perform paired *t*-tests for electrophysiological data and one way ANOVAs for RT-qPCR data.

Results

Motor neurons identically express myosuppressin receptor subtypes

Single cell RT-qPCR was performed to examine the expression of myosuppressin receptor subtypes in individual motor neurons pulled from the CG (see Methods). All pulled cells expressed 18S mRNA at the same level (Figure 5B), indicating that individual neurons were successfully isolated. Thus, all cells were used for single-cell qPCR using MSRI and MSRII primers. On average, the C_q values for MSRI were 33 across all large cells, and the C_q values for MSRII were 27 across all large cells (Figure 5C, D). There were no significant differences between large cell types, indicating that each large cell expressed MSRI and MSRII at the same level. Because each PCR cycle doubles the amount of target sequence, MSRII

expression was 60-fold higher than MSRI expression. MSRII and 18S C_q values had a significantly positive relationship (R^2=0.2057, P=0.01040), indicating that cells with more mRNA contained more of each transcript (Figure 6A). There was no significant correlation between MSRI and 18S C_q values (R^2=0.005325). This result indicated that electrophysiological responses to myosuppressin should be the same across motor neurons.

Raw C_q values were used to compare between LCs because the amount of mRNA in each sample was experimental normalized; we were confident that each sample contained one cell's worth of DNA, and that any variability seen in those measurements was due to cell-to-cell variability. Previous work from the lab of David Schulz, with whom this work was performed, has shown that raw cycle quantification values are sufficient to detect mRNA correlation in large cells from the *Cancer borealis* cardiac ganglion (Tobin et al., 2009). As a precaution, however, we also compared fold change in MSRII expression using the $2^{-\Delta\Delta Cq}$ method, using 18S as a reference gene and LC1 as an arbitrary control condition. There was no difference in expression between any of the five motor neurons (Figure 6B).

Myosuppressin decreases burst frequency and the rate of depolarization during the interburst interval

Sharp intracellular recordings were used to investigate the modulatory effect of myosuppressin on motor neuron output. Myosuppressin (10^{-6} M) was superfused over the intact CG and elicited a sharp decrease in burst frequency, as expected from previous studies. However, unlike previous studies, there was no decrease in the afterhyperpolarization (Figure 7). The most drastic change in motor neuron activity occurred during the inter-burst interval, where the rate of change of depolarization (*dV/dt*) significantly decreased (P=0.0143, paired t-test). Because we were not injecting any current, we assumed that the following relation held true for

these neurons: $I_{net}=C*(dV/dt)$, where C is membrane capacitance. Thus, we deduced that myosuppressin altered neuronal activity by either increasing the magnitude of outward current or decreasing the magnitude of inward current during the inter-burst interval.

Myosuppressin modulation is eliminated after the application of TTX

If myosuppressin modulated a subthreshold current like leak or persistent sodium, it should change the resting membrane potential in a quiescent cell. Sharp electrode intracellular recordings were used to determine if myosuppressin altered the resting membrane potential in the absence of bursting activity (Figure 8). Cells were bathed in TTX (10^{-7} M) to eliminate bursting. There was no major change in resting membrane potential from saline baseline to myosuppressin (10^{-6} M) (n=4; Figure 8).

Myosuppressin perturbs the normal membrane potential waveform

In some cases (n=4 out of 6), myosuppressin (10^{-6} M) increased the burst duration in motor neurons during sharp intracellular recordings (Figure 9A). Bursts decayed rapidly, then remained in a plateau state longer than during baseline (Figure 9A). On one occasion, myosuppressin elicited multiple bouts of prolonged excitation in the motor neuron (Figure 9B). This prolonged depolarization typically occurred immediately after a burst, suggesting that the currents underlying the plateau potential failed to inactivate, or that the burst failed to terminate. Each prolonged depolarization was accompanied by tonic spiking and short bursts of action potentials. All cells eventually returned to baseline (Figure 9).

Myosuppressin does not alter peak outward current

To determine if myosuppressin alters outward currents in CG motor neurons, we used two-electrode voltage clamp to directly measure current during a set of depolarizing voltage steps from -90 mV to 0 mV (n=3; Figure 10). Outward currents occurred in two phases: a

transient outward current in the first 500 ms followed by a steady-state outward current. This current was apparent starting at -40 mV (Figure 11). At command voltage values above -20 mV, the voltage failed to clamp at a steady value; instead, it wobbled at different voltages before reaching a steady voltage value (Figure 10). For this reason, only clamps from -90 mV to -20 mV were averaged and analyzed (Figure 13). From -90 mV to about -60 mV, there was no transient peak in outward current; instead, outward current was steady for the duration of the step.

We plotted peak outward current in saline and in myosuppressin normalized to the maximum peak current in saline (n=3; Figure 13A). We also plotted the steady-state component of the outward current normalized to the maximum steady-state outward current (Figure 13B). The reversal potential for peak outward current hovered near -60 mV, while the reversal potential for steady state outward current hovered near -50 mV (Figure 13). From about -90 mV to -60 mV, total outward current increased linearly (Figure 13A). From about -60 mV to -20 mV, total outward current increased nonlinearly (Figure 13A). There was no shift in voltage dependence for either the steady state or peak outward current. The slope of the IV curve for peak outward current did not substantially change after treatment with myosuppressin. For the steady-state outward current, the slope slightly increased in myosuppressin (Figure 13B).

Discussion

The results from this study indicated that motor neurons in the CG are likely modulated by myosuppressin. They expressed appreciable amounts of MSRII, and myosuppressin robustly decreased burst frequency and the rate of depolarization during the interburst interval. Surprisingly, however, peak outward current was unaffected by myosuppressin, as indicated by two-electrode voltage clamp experiments. Future studies should focus on parsing out the total

outward current, including measuring the peak amplitude and kinetics of specific currents like I_A and I_{KCa}. Peak current is only one parameter in ion channel function. Theoretical studies of model oscillating neurons show that altering ion channel kinetics can also result in profound changes in electrical output (Oh et al., 2012). The results presented here suggest that subtle changes in membrane properties likely cause the drastic change in neural output during modulation by myosuppressin. The CG is multiply modulated; understanding the arsenal of modulatory targets available in this simple neural circuit will provide a broader understanding of how behaviorally relevant neural circuit output is regulated.

Myosuppressin receptors are expressed equally in all motor neurons

Our study is the first to quantitatively characterize the expression of myosuppressin receptors in the motor neurons of the CG. Previous research has demonstrated that MSR subtypes I through V are present in the lobster nervous system, with MSRII through IV enriched in the lobster CG (Oleisky et al., 2020). In RT-PCR of lobster CG, MSRII is preferentially expressed in the large cells, while MSRIII and MSRIV were expressed in small cells, supporting the hypothesis that myosuppressin elicits cell-type specific effects on the CG circuit (Oleisky et al., 2020). However, tissue-level RT-qPCR data from a collaborator suggests that MSRI and MSRII are the most highly expressed myosuppressin receptors in the CG (Schulz D., personal communication). We found that the expression of MSRII in CG motor neurons was 60-fold greater than the expression of MSRI, supporting the idea that the expression of MSRII is exclusive to the motor neurons. The C_q values obtained for MSRI suggest that it may even be absent from the cells entirely. After that many cycles of PCR, amplification of some nucleic acid is bound to occur. The possibility that the motor neuron response to myosuppressin is shaped by

a single, organizing motor neuron was ruled out by the fact that all cells expressed MSRII at the same level.

Our RT-qPCR results also contribute to a growing literature on cell identity in crustacean and mammalian neural circuits. It has been suggested that the LCs in crustacean CGs are largely identical; however, they differ slightly in their synaptic connections and physiology (Hartline, 1979). In *H. americanus,* the expression of ion channel genes does not vary between cell types; included among the ion channels with substantial expression is *Shaker*, which passes A-type potassium current (Schulz, D.J., personal communication). Within-animal variability of ion channel expression was not addressed in our study; however, ion channel mRNA correlations reveal that LCs from crab CGs are just as similar within animals as they are across animals (Tobin et al., 2009). Thus, the variability seen in MSRII expression in LCs across animals in our study are likely the same as the variability of different motor neurons within each animal. In other words, LCs are the same within and across animals.

The identity of cells at the molecular level (especially regarding the expression of ion channels) is important for how they are modulated. Ion channel mRNA expression levels tightly correlate with ionic current density (Schulz et al., 2006). In a comparison between currents in a population of biophysical models of the *Cancer borealis* CG and ion channel mRNA values from individual CG neurons, *NALCN/*I_{NaP} and *IRK/*I_{Leak} were the most tightly correlated in both realms (Dopp et al., 2021, preprint). Thus, models and biological systems tightly regulate the expression and conductance magnitude of two important subthreshold currents; perturbations in this relationship may underly the consistent effect elicited by myosuppressin the lobster CG. In the near future, the samples from this study could be used for qPCR experiments with a cassette of different ion channel primers. This would quickly tell us if the cells were all in the proper region

of ion channel space to be easily tuned by myosuppressin. If they reside in a region of conductance space adjacent to a region of slower bursting, a slight nudge by myosuppressin could be sufficient to alter neuronal output. Given how consistently myosuppressin alters burst activity, this prediction may hold true.

Myosuppressin alters the electrophysiological properties of the cardiac ganglion

We first used sharp intracellular recordings to test how myosuppressin might affect the membrane potential waveform of LCs in the intact, bursting CG. Our results indicated that myosuppressin invariably decreased burst frequency in the CG, in concert with past research (Stevens et al., 2009; Oleisky et al., 2020, 2022). The rate of depolarization decreased during the inter-burst interval. Assuming that the neuronal membrane during intracellular recording function as an *RC* circuit, the relationship between current and voltage across the membrane is $I_{net} = C\frac{dV}{dt}$; this implies that the net inward current decreased after treatment with myosuppressin (Hodgkin et al., 1952). Various subthreshold currents are implicated during the interburst interval, including A-type potassium current, H-current, and persistent sodium current. Of these, only A-type potassium current has been recorded in these neurons, which made it a prime candidate for further electrophysiological study.

We failed to observe a decrease in the afterhyperpolarization, in contrast to previous findings (Stevens et al., 2009). Afterhyperpolarizations hovered near -50 mV on average in our experiments; in previous studies where myosuppressin enhanced afterhyperpolarizations, this value was closer to -60 mV (Stevens et al., 2009). One explanation for this discrepancy is that the membrane health of our preps differed and as a result were more depolarized than normal. If myosuppressin enhanced an inward rectifier current, we may have avoided seeing this effect by being outside the voltage-dependent range of the inward rectifier. Because the *Drosophila*

myosuppressin receptor is G_i-coupled, myosuppressin could activate GIRK channels (Dascal and Kahanovitch, 2015). This phenomenon is observed in bursting mammalian thalamocortical cells; depolarizations render some currents inactive (McCormick and Pape, 1990). However, the extensive literature on *H. americanus* CG physiology suggests that healthy motor neurons have a resting membrane potential at about -50 mV, which was true of all experiments analyzed in this study (Cooke, 2002b). Thus, all the cells in our study had healthy membranes. Alternatively, the cells in our study may have differed such that baseline burst frequency differed. In LP neurons in the crab stomatogastric ganglion, the amplitude of a proctolin-induced inward current depends on cycle frequency (Schneider et al., 2021).

In some of our experiments, myosuppressin elicited either longer bursts or prolonged depolarization that disappeared during the wash period (Figure 9). This depolarization was accompanied by tonic action potentials and small bursts. Though uncommon, it happened more than once and hints at the action of myosuppressin. If myosuppressin targets calcium-dependent potassium channels, a decrease in calcium sensitivity or peak conductance could cause the burst to fail to terminate. If calcium currents are not being opposed by strong, calcium-dependent potassium currents, then decay back to resting membrane potential would depend on the slow inactivation of calcium currents. Curiously, driver potential-mediated bursts were seen during this prolonged excitation. It is possible that the prolonged depolarization was caused by the enhancement of a previously undescribed slow, non-inactivating inward current in cardiac ganglion motor neurons. Another explanation is that the synaptic drive onto large motor neurons is targeted by myosuppressin. If excitatory synapses from small cells are more active than normal, they may sustain a depolarization in the large cells that is independent of the calcium-mediated driver potential. However, we did not observe barrages of synaptic potentials when this

sustained depolarization occurred. It is strange that myosuppressin would somehow enhance depolarization, given its drastic slowing of the burst frequency and rate of depolarization in the interburst interval. Overall, myosuppressin may be targeting multiple currents in the cardiac ganglion; this is not an uncommon mechanism for modulator action (Marder and Bucher, 2007). If it enhances A-type potassium current in the interburst interval and decreases calcium-dependent potassium current at the end of the driver potential, the net effect of myosuppressin on total outward current may appear negligible.

Myosuppressin produces a remarkably consistent change in network activity in the cardiac ganglion, more so than some other peptide modulators in the crustacean nervous system (Dickinson et al., 2018). This is surprising considering the high variability across animals in absolute ion channel expression levels (Schulz et al., 2006). Inter-animal ion channel expression in the same neuron type from the crab stomatogastric ganglion is highly variable (Schulz et al., 2007). Models of intrinsically bursting LP neurons in the crab stomatogastric nervous system reveals that sets of ionic conductance values may even sit in a favorable region of conductance space for rhythmicity, following only weak correlations (Taylor et al., 2009). Perturbations to the balance of ion channel conductances often produce inconsistent effects on circuit output because of this variability (Goaillard and Marder, 2021). The effects of modulatory molecules also depend on previous modulatory history (Lett et al., 2017). Thus, the effects of neuropeptides on the lobster cardiac system depend on multiple variable factors, including the expression of peptide receptors and the maximal conductance values for target current types. The qPCR results from earlier suggested that all LCs should respond to myosuppressin. The network-level changes in output reported in this subsection suggest that in all samples, something is changing that always causes a decrease in burst frequency and depolarization. Both frequency and rate of

change are continuous variables, so changes in one membrane current property, like A-type potassium current, could cause a decrease in these properties on a sliding scale. Slowing down the rhythm of the CG is relatively easy task for a modulator versus changing the state of neural output (like a switch from tonic firing to bursting).

Total outward current does not change in response to myosuppressin

We used two-electrode voltage clamp to investigate how outward currents are modulated by myosuppressin. Recordings of total outward currents indicated that there were two main components: one transient, likely representing A-type potassium current, and one steady state, likely representing leak current, delayed-rectifier, and calcium-dependent potassium current (Figure 11, 12). This matches previous reports of membrane currents in *H. americanus* large cells (Tazaki and Cooke, 1986).

The current-voltage relationship of outward currents in LCs did not differ between saline and myosuppressin superfusion (Figure 13). The reversal potential for peak outward current was near -60 mV, indicating that this outward current is mostly carried by potassium ions. The reversal potential for leak currents was also hyperpolarized but was closer to -55 mV. Because we examined only *total* current, our data represented all outward currents, including leak and I_A. The simplest prediction for myosuppressin modulation, made earlier, is that myosuppressin increases the conductance magnitude of A-type potassium channels, causing stronger hyperpolarization during the inter-burst interval, decreased net inward current, a slower rate of depolarization, and decreased burst frequency. The current-voltage plots for outward currents, however, contradict this idea. The voltage-dependence did not substantially vary between experimental conditions for either the peak or steady state outward current components. This is especially true at command voltages that mimic the membrane potential during the inter-burst

interval (-60 mV to -40 mV); in saline and myosuppressin, the current magnitudes were identical. It is therefore unlikely that myosuppressin alters the amount of ionic current that passes through A-type potassium channels; nor is it likely that myosuppressin induces an increase in membrane A-type potassium channel density.

There are various speculative explanations for why no substantial changes in outward current were observed in LCs, despite such robust network responses. It is possible that we faced space-clamp issues that precluded us from observing changes in subthreshold membrane currents that may be changing in other regions of the cell. Crustacean motor neurons are big cells, and may have distinct electrical compartments. Some studies have shown that neurons in the crustacean stomatogastric ganglion are electrotonically compact, despite complex branching morphologies (Otopalik et al., 2017). It was clear from our recordings, however, that we were far from the spike initiation zone; substantial spatial decay occurred that made action potentials appear as small blips above the larger drive potential (Figure 7, 9). Modeling studies of the crab CG suggest that the spike initiation zone in the proximal axon contains persistent sodium current and calcium-dependent potassium current (Dopp et al., 2021, preprint); if the ion channels being modulated by myosuppressin are far from the recording site, then they may decay over space and not get picked up in our two-electrode voltage clamp experiments. The driver potential itself arises from the axon trigger zone, meaning that calcium channels and, presumably, potassium-dependent calcium channels, are localized there (Cooke, 2002b). Dopamine and serotonin exert their excitatory effects on SC activity in *H. americanus* from axonal processes alone, indicating that local depolarizations near the spike initiation zone may be sufficient to change activity (Berlind, 1998). If myosuppressin caused changes to synapses or electrotonically separate compartments in LCs to elicit a change in circuit output, they would not be observable in two-

electrode voltage clamp. Excitatory feedback from LCs onto SCs can also influence burst frequency and duration; elimination of this feedback causes SC burst frequency to increase (Mayeri, 1973). It is possible that myosuppressin modulates this feedback, thus limiting the effects to synaptic mechanisms on the SCs. However, if this were the case, then myosuppressin modulation of LC burst frequency would depend on coupling to the SCs; experiments by Oleisky and colleagues indicate that myosuppressin modulates LCs even in the absence of SC input (Oleisky et al., 2020).

CG neurons in *H. americanus* also express a variety of innexin and gap junction proteins, which may themselves be targeted for modulation (Christie et al., 2020). Usually, modulating innexin proteins results in changes to synchrony among the connected neurons. For example, dopamine modulates innexin strength in the crab CG to maintain synchronous output after a perturbation to a single channel that disrupts coordinated circuit output (Lane et al., 2016b, 2018). The motor neurons of the CG are electrotonically coupled; regulation of this coupling may confer unique control over the integration of synaptic signals via the filtering capabilities of electrotonic connections between neurons. The electrical synapses among LCs and between LCs and SCs function as low-pass filters and can influence the timing of small cell pacemaking (Hartline, 1979). Thus, modulation of electrical synapses could possibly underlie the change in burst frequency seen in response to myosuppressin.

One can speculate that myosuppressin more subtly alters neural activity by changing how motor neurons process information from inputs and intrinsically active subthreshold currents. Subthreshold leak currents and persistent sodium currents in mouse respiratory centers operate over a wide range of conductance values to control oscillatory activity (Koizumi and Smith, 2008). These may be useful dials to tune CPG oscillatory frequency. These channels are not

uncommonly modulated; in rhythmically firing dopamine neurons in the mouse ventral tegmental area, auto-signaling dopamine activates a G_i-coupled receptor and decreases the amplitude of persistent sodium carried by the channel NALCN (Philippart and Khaliq, 2018). A change in subthreshold leak currents can also alter the resistance of the membrane, which would subsequently change how inputs from the pacemaker cells depolarize the membrane. We would expect a change in these currents to cause a change in resting membrane potential during quiescence; however, we observed no changes to resting membrane potential in LCs bathed in TTX. (Figure 8). Thus, this possibility is unlikely.

Future directions

The two-electrode voltage clamp data represent total outward current; going forward, students interested in following-up this project should perform more finely tuned voltage clamp experiments to isolate specific currents like I_A (Figure 14). Holding at -90 mV elicits total outward current and holding at-40 mV elicits total outward current minus I_A, because I_A inactivates at -40 mV. Subtracting current traces would thus allow students to isolate I_A. If myosuppressin has opposing effects on two different potassium currents in the same neuron, separating the different potassium currents would be imperative for observing the actual effects of myosuppressin. Measuring only total outward current might occlude more complicated phenomena during modulation by myosuppressin.

To test if changes in I_{KCa} occur in myosuppressin, future students should perform a similar voltage protocol (Figure 15). Students could hold the membrane potential at -90 mV for 1000 ms then step from -90 mV to 0 mV in increments of +10 mV to elicit total outward current for both physiological saline and myosuppressin. Then, they could perform the same protocol in the presence of cadmium ions. Cadmium ions block calcium channels. Thus, current traces

obtained in cadmium contain all outward currents except I_{KCa}. Subtracting the current traces would thus allow them to isolate I_{KCa}.

If I_A is not targeted by myosuppressin, students could investigate other possible modulatory mechanisms. It is possible that I_{KCa} kinetics change to alter LC bursting. To test for changes in channel kinetics, we would use exponential curves fit to each current. Finally, we can investigate the effects of myosuppressin other subthreshold currents that may be present in the motor neurons of the CG. It would be relatively easy to establish the presence of a persistent sodium current using a pharmacological blocker I_{NaP}; once a persistent sodium current is identified, it can be manipulated in tandem with myosuppressin treatment to test if myosuppressin acts on it. Myosuppressin may also change non-cell intrinsic function, like synaptic transmission from small cells. A change in the membrane properties of the cell may make it more difficult to depolarize during the interburst interval, without causing an obvious change in total outward current. This includes decreasing the input resistance of the neurons, perhaps through altering the conductance of leak channels. Further work should explore these possibilities. Ultimately, understanding how the peptidergic signaling system in the lobster will contribute to our understanding of how rhythmic neural circuit output can be changed at the level of ionic membrane currents. This will inform our understanding of behaviors like sleep, reward, and a myriad of others that operate on the same basic principles of neural oscillation and modulation.

References

Alonso LM, Marder E (2019) Visualization of currents in neural models with similar behavior and different conductance densities. eLife 8:e42722.

Amendola J, Woodhouse A, Martin-Eauclaire M-F, Goaillard J-M (2012) Ca2+/cAMP-Sensitive Covariation of IA and IH Voltage Dependences Tunes Rebound Firing in Dopaminergic Neurons. Journal of Neuroscience 32:2166–2181.

An WF, Bowlby MR, Betty M, Cao J, Ling H-P, Mendoza G, Hinson JW, Mattsson KI, Strassle BW, Trimmer JS, Rhodes KJ (2000) Modulation of A-type potassium channels by a family of calcium sensors. Nature 403:553–556.

Bass C, Katanski C, Maynard B, Zurro I, Mariane E, Matta M, Loi M, Melis V, Capponi V, Muroni P, Setzu M, Nichols R (2014) Conserved residues in RF-NH2 receptor models identify predicted contact sites in ligand–receptor binding. Peptides 53:278–285.

Berlind A (1993) Heterogeneity of motoneuron driver potential properties along the anterior-posterior axis of the lobster cardiac ganglion. Brain Res 609:51–58.

Berlind A (1998) Dopamine and 5-hydroxytryptamine actions on the cardiac ganglion of the lobster Homarus americanus. Journal of Comparative Physiology A: Sensory, Neural, and Behavioral Physiology 182:363–376.

Bourdeau ML, Morin F, Laurent CE, Azzi M, Lacaille J-C (2007) Kv4.3-Mediated A-Type K+ Currents Underlie Rhythmic Activity in Hippocampal Interneurons. Journal of Neuroscience 27:1942–1953.

Christie AE, Chi M, Lameyer TJ, Pascual MG, Shea DN, Stanhope ME, Schulz DJ, Dickinson PS (2015) Neuropeptidergic Signaling in the American Lobster Homarus americanus: New Insights from High-Throughput Nucleotide Sequencing Johnson EC, ed. PLoS ONE 10:e0145964.

Christie AE, Hull JJ, Dickinson PS (2020) In silico analyses suggest the cardiac ganglion of the lobster, Homarus americanus, contains a diverse array of putative innexin/innexin-like proteins, including both known and novel members of this protein family. Invert Neurosci 20:5.

Clerx M, Beattie KA, Gavaghan DJ, Mirams GR (2019) Four Ways to Fit an Ion Channel Model. Biophys J 117:2420–2437.

Connor JA, Stevens CF (1971a) Voltage clamp studies of a transient outward membrane current in gastropod neural somata. The Journal of Physiology 213:21–30.

Connor JA, Stevens CF (1971b) Prediction of repetitive firing behaviour from voltage clamp data on an isolated neurone soma. The Journal of Physiology 213:31–53.

Cooke IM (2002a) Reliable, responsive pacemaking and pattern generation with minimal cell numbers: the crustacean cardiac ganglion. Biol Bull 202:108–136.

Cooke IM (2002b) Reliable, responsive pacemaking and pattern generation with minimal cell numbers: the crustacean cardiac ganglion. Biol Bull 202:108–136.

Dascal N, Kahanovitch U (2015) The Roles of Gβγ and Gα in Gating and Regulation of GIRK Channels. Int Rev Neurobiol 123:27–85.

Dickinson PS, Armstrong MK, Dickinson ES, Fernandez R, Miller A, Pong S, Powers BW, Pupo-Wiss A, Stanhope ME, Walsh PJ, Wiwatpanit T, Christie AE (2018) Three members of a peptide family are differentially distributed and elicit differential state-dependent responses in a pattern generator-effector system. Journal of Neurophysiology 119:1767–1781.

Dickinson PS, Mecsas C, Marder E (1990) Neuropeptide fusion of two motor-pattern generator circuits. Nature 344:155–158.

Egerod K, Reynisson E, Hauser F, Cazzamali G, Williamson M, Grimmelikhuijzen CJP (2003) Molecular cloning and functional expression of the first two specific insect myosuppressin receptors. Proceedings of the National Academy of Sciences 100:9808–9813.

Franklin CC, Ball JM, Schulz DJ, Nair SS (2010) Generation and Preservation of the Slow Underlying Membrane Potential Oscillation in Model Bursting Neurons. Journal of Neurophysiology 104:1589–1602.

Goaillard J-M, Marder E (2021) Ion Channel Degeneracy, Variability, and Covariation in Neuron and Circuit Resilience. Annu Rev Neurosci 44:335–357.

Golowasch J, Abbott LF, Marder E (1999) Activity-dependent regulation of potassium currents in an identified neuron of the stomatogastric ganglion of the crab Cancer borealis. J Neurosci 19:RC33.

Golowasch J, Buchholtz F, Epstein IR, Marder E (1992) Contribution of individual ionic currents to activity of a model stomatogastric ganglion neuron. Journal of Neurophysiology 67:341–349.

Golowasch J, Marder E (1992) Proctolin activates an inward current whose voltage dependence is modified by extracellular Ca2+. J Neurosci 12:810–817.

Harris-Warrick RM, Coniglio LM, Levini RM, Gueron S, Guckenheimer J (1995) Dopamine modulation of two subthreshold currents produces phase shifts in activity of an identified motoneuron. J Neurophysiol 74:1404–1420.

Harris-Warrick RM, Flamm RE (1987) Multiple mechanisms of bursting in a conditional bursting neuron. Journal of Neuroscience 7:2113–2128.

Hartline DK (1979) Integrative Neurophysiology of the Lobster Cardiac Ganglion. Am Zool 19:53–65.

Hodgkin AL, Huxley AF, Katz B (1952) Measurement of current-voltage relations in the membrane of the giant axon of *Loligo*. The Journal of Physiology 116:424–448.

Hooper SL, Thuma JB, Guschlbauer C, Schmidt J, Büschges A (2015) Cell dialysis by sharp electrodes can cause nonphysiological changes in neuron properties. Journal of Neurophysiology 114:1255–1271.

Johnson EC, Bohn LM, Barak LS, Birse RT, Nässel DR, Caron MG, Taghert PH (2003) Identification of Drosophila Neuropeptide Receptors by G Protein-coupled Receptors-β-Arrestin2 Interactions. Journal of Biological Chemistry 278:52172–52178.

Koizumi H, Smith JC (2008) Persistent Na+ and K+-Dominated Leak Currents Contribute to Respiratory Rhythm Generation in the Pre-Botzinger Complex In Vitro. Journal of Neuroscience 28:1773–1785.

Kryshtal' DO, Nesin VV, Shuba MF (2007) Modulation of A-type potassium current in smooth-muscle cells of the rat Vas Deferens by Ca2+/calmodulin-dependent protein kinase II. Neurophysiology 39:369–372.

Lane BJ, Lane BJ, Kick DR, Wilson DK, Nair SS, Schulz DJ, Schulz DJ (2018) Dopamine maintains network synchrony via direct modulation of gap junctions in the crustacean cardiac ganglion. eLife 7.

Lane BJ, Samarth P, Ransdell JL, Nair SS, Schulz DJ (2016a) Synergistic plasticity of intrinsic conductance and electrical coupling restores synchrony in an intact motor network. eLife 5.

Lane BJ, Samarth P, Ransdell JL, Nair SS, Schulz DJ (2016b) Synergistic plasticity of intrinsic conductance and electrical coupling restores synchrony in an intact motor network. eLife 5.

Leander M, Bass C, Marchetti K, Maynard BF, Wulff JP, Ons S, Nichols R (2015) Cardiac Contractility Structure-Activity Relationship and Ligand-Receptor Interactions; the Discovery Of Unique and Novel Molecular Switches in Myosuppressin Signaling Lee LTO, ed. PLoS ONE 10:e0120492.

Lett KM, Garcia VJ, Temporal S, Bucher D, Schulz DJ (2017) Removal of endogenous neuromodulators in a small motor network enhances responsiveness to neuromodulation. Journal of Neurophysiology 118:1749–1761.

Livak KJ, Schmittgen TD (2001) Analysis of relative gene expression data using real-time quantitative PCR and the 2(-Delta Delta C(T)) Method. Methods 25:402–408.

MacLean JN, Zhang Y, Johnson BR, Harris-Warrick RM (2003) Activity-Independent Homeostasis in Rhythmically Active Neurons. Neuron 37:109–120.

Marder E, Bucher D (2001) Central pattern generators and the control of rhythmic movements. Curr Biol 11:R986-96.

Marder E, Bucher D (2007) Understanding Circuit Dynamics Using the Stomatogastric Nervous System of Lobsters and Crabs. Annu Rev Physiol 69:291–316.

Marder E, O'Leary T, Shruti S (2014) Neuromodulation of Circuits with Variable Parameters: Single Neurons and Small Circuits Reveal Principles of State-Dependent and Robust Neuromodulation. Annu Rev Neurosci 37:329–346.

Mayeri E (1973) Functional Organization of the Cardiac Ganglion of the Lobster, Homarus americanus. J Gen Physiol 62:448–472.

Maynard BF, Bass C, Katanski C, Thakur K, Manoogian B, Leander M, Nichols R (2013) Structure-Activity Relationships of FMRF-NH2 Peptides Demonstrate A Role for the Conserved C Terminus and Unique N-Terminal Extension in Modulating Cardiac Contractility Uversky VN, ed. PLoS ONE 8:e75502.

McCormick DA, Pape HC (1990) Properties of a hyperpolarization-activated cation current and its role in rhythmic oscillation in thalamic relay neurones. The Journal of Physiology 431:291–318.

Nässel DR (2002) Neuropeptides in the nervous system of Drosophila and other insects: multiple roles as neuromodulators and neurohormones. Progress in Neurobiology 68:1–84.

Nichols R (1992) Isolation and Structural Characterization of Drosophila TDVDHVFLRFamide and FMRFamide-Containing Neural Peptides. J Mol Neurosci 3:213–218.

Nusbaum MP, Blitz DM (2012) Neuropeptide modulation of microcircuits. Curr Opin Neurobiol 22:592–601.

Nusbaum MP, Blitz DM, Marder E (2017) Functional consequences of neuropeptide and small-molecule co-transmission. Nat Rev Neurosci 18:389–403.

Oh M, Zhao S, Matveev V, Nadim F (2012) Neuromodulatory changes in short-term synaptic dynamics may be mediated by two distinct mechanisms of presynaptic calcium entry. J Comput Neurosci 33:573–585.

O'Leary T, Williams AH, Caplan JS, Marder E (2013) Correlations in ion channel expression emerge from homeostatic tuning rules. Proceedings of the National Academy of Sciences 110:E2645–E2654.

Oleisky ER, Stanhope ME, Hull JJ, Christie AE, Dickinson PS (2020) Differential neuropeptide modulation of premotor and motor neurons in the lobster cardiac ganglion. Journal of Neurophysiology 124:1241–1256.

Oleisky ER, Stanhope ME, Hull JJ, Dickinson PS (2022) Isoforms of the neuropeptide myosuppressin differentially modulate the cardiac neuromuscular system of the American lobster, *Homarus americanus*. Journal of Neurophysiology 127:702–713.

Otopalik AG, Sutton AC, Banghart M, Marder E (2017) When complex neuronal structures may not matter. eLife 6:e23508.

Philippart F, Khaliq ZM (2018) Gi/o protein-coupled receptors in dopamine neurons inhibit the sodium leak channel NALCN. eLife 7:e40984.

Powers KG, Ma X-M, Eipper BA, Mains RE (2019) Identifying roles for peptidergic signaling in mice. Proc Natl Acad Sci USA 116:20169–20179.

Prinz AA, Bucher D, Marder E (2004) Similar network activity from disparate circuit parameters. Nature Neuroscience 7:1345–1352.

Ransdell JL, Temporal S, West NL, Leyrer ML, Schulz DJ (2013) Characterization of inward currents and channels underlying burst activity in motoneurons of crab cardiac ganglion. Journal of Neurophysiology 110:42–54.

Santin JM, Schulz DJ (2019) Membrane Voltage Is a Direct Feedback Signal That Influences Correlated Ion Channel Expression in Neurons. Current Biology 29:1683-1688.e2.

Schneider AC, Fox D, Itani O, Golowasch J, Bucher D, Nadim F (2021) Frequency-Dependent Action of Neuromodulation. eNeuro 8:ENEURO.0338-21.2021.

Schulz DJ, Goaillard J-M, Marder E (2006) Variable channel expression in identified single and electrically coupled neurons in different animals. Nature Neuroscience 9:356+.

Schulz DJ, Goaillard J-M, Marder EE (2007) Quantitative expression profiling of identified neurons reveals cell-specific constraints on highly variable levels of gene expression. Proceedings of the National Academy of Sciences 104:13187–13191.

Stemmler EA, Cashman CR, Messinger DI, Gardner NP, Dickinson PS, Christie AE (2007) High-mass-resolution direct-tissue MALDI-FTMS reveals broad conservation of three neuropeptides (APSGFLGMRamide, GYRKPPFNGSIFamide and pQDLDHVFLRFamide) across members of seven decapod crustaean infraorders. Peptides 28:2104–2115.

Stevens JS, Cashman CR, Smith CM, Beale KM, Towle DW, Christie AE, Dickinson PS (2009) The peptide hormone pQDLDHVFLRFamide (crustacean myosuppressin) modulates the Homarus americanus cardiac neuromuscular system at multiple sites. Journal of Experimental Biology 212:3961–3976.

Swensen AM, Marder E (2000) Multiple peptides converge to activate the same voltage-dependent current in a central pattern-generating circuit. J Neurosci 20:6752–6759.

Swensen AM, Marder E (2001) Modulators with convergent cellular actions elicit distinct circuit outputs. J Neurosci 21:4050–4058.

Taylor AL, Goaillard J-M, Marder E (2009) How Multiple Conductances Determine Electrophysiological Properties in a Multicompartment Model. Journal of Neuroscience 29:5573–5586.

Tazaki K, Cooke IM (1986) Currents under voltage clamp of burst-forming neurons of the cardiac ganglion of the lobster (Homarus americanus). J Neurophysiol 56:1739–1762.

Tazaki K, Cooke IM (1990) Characterization of Ca current underlying burst formation in lobster cardiac ganglion motorneurons. Journal of Neurophysiology 63:370–384.

Tobin A-E, Cruz-Bermúdez ND, Marder E, Schulz DJ (2009) Correlations in Ion Channel mRNA in Rhythmically Active Neurons Brezina V, ed. PLoS ONE 4:e6742.

Turrigiano GG, Nelson SB (2004) Homeostatic plasticity in the developing nervous system. Nat Rev Neurosci 5:97–107.

Varoqueaux F, Williams EA, Grandemange S, Truscello L, Kamm K, Schierwater B, Jékely G, Fasshauer D (2018) High Cell Diversity and Complex Peptidergic Signaling Underlie Placozoan Behavior. Current Biology 28:3495-3501.e2.

Williams AH, Calkins A, O'Leary T, Symonds R, Marder E, Dickinson PS (2013a) The Neuromuscular Transform of the Lobster Cardiac System Explains the Opposing Effects of a Neuromodulator on Muscle Output. Journal of Neuroscience 33:16565–16575.

Williams AH, Kwiatkowski MA, Mortimer AL, Marder E, Zeeman ML, Dickinson PS (2013b) Animal-to-animal variability in the phasing of the crustacean cardiac motor pattern: an experimental and computational analysis. J Neurophysiol 109:2451–2465.

Witzel K, Fischer P, Bähring R (2012) Hippocampal A-type current and Kv4.2 channel modulation by the sulfonylurea compound NS5806. Neuropharmacology 63:1389–1403.

Yuste R, MacLean JN, Smith J, Lansner A (2005) The cortex as a central pattern generator. Nat Rev Neurosci 6:477–483.

Figures

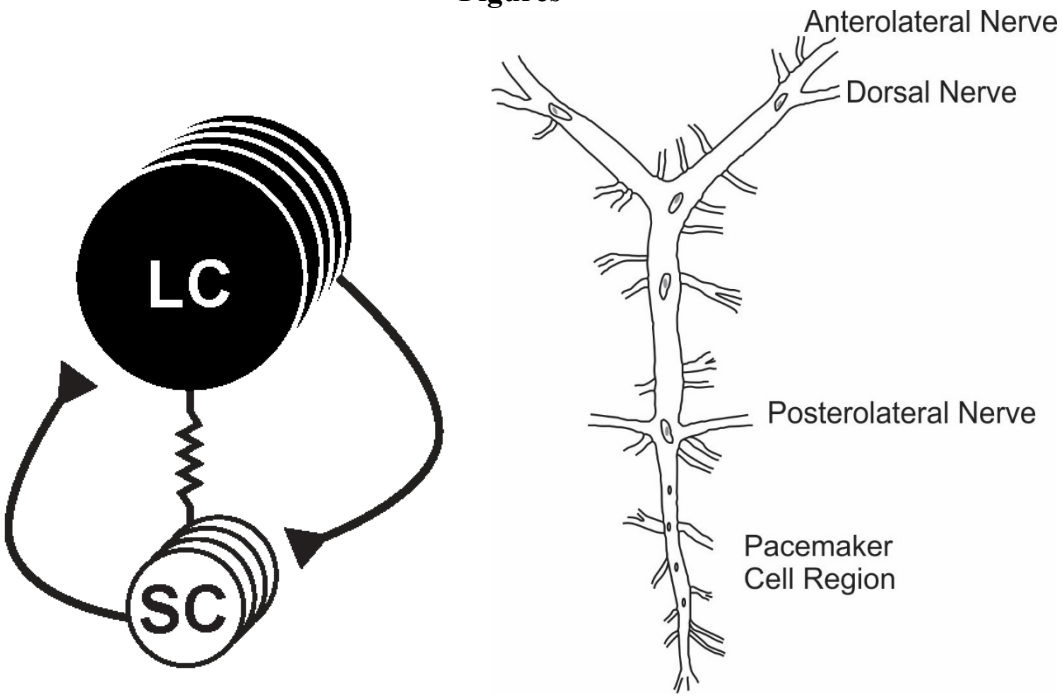

Figure 1. Schematic of the lobster cardiac ganglion after it has been removed from cardiac musculature. The posterior region contains pacemaker neurons, and the anterior region contains motor neurons. In all electrophysiological experiments, the anterolateral nerve was desheathed to expose either LC1, LC2, or LC3.

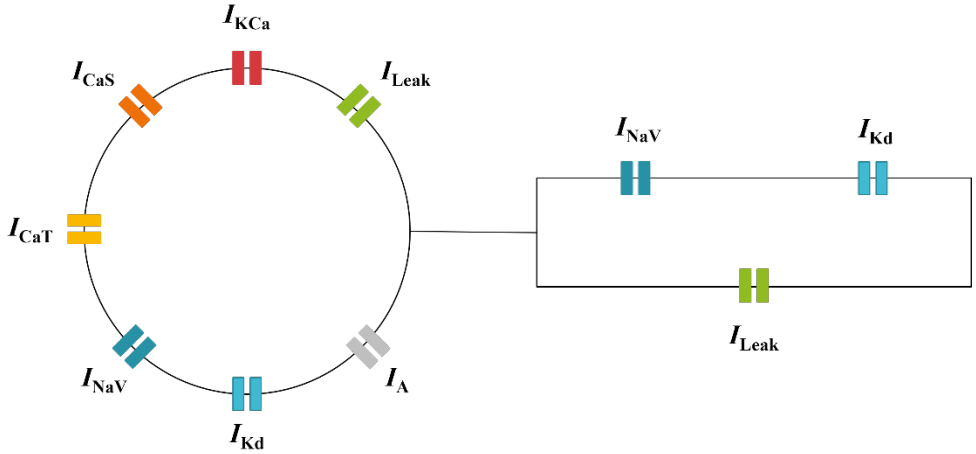

Figure 2. Schematic of the ion channels responsible for the driver potential and spiking activity in cardiac ganglion large cells. The cell is separated into two distinct compartments: the soma and proximal axon, and the distal axon. The soma and proximal axon contain subthreshold currents responsible for the driver potential. The distal axon contains currents responsible for fast spiking.

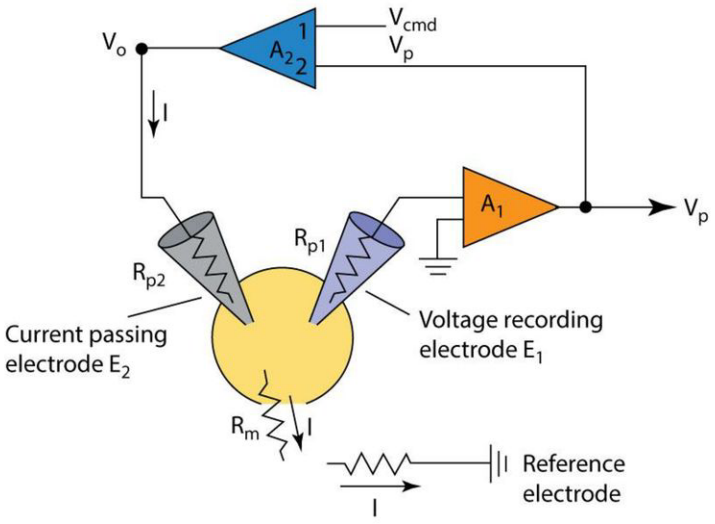

Figure A4.4 Two-electrode voltage clamp.
Adapted from The Axon Guide, Axon Instruments Inc., 1993.

34

Figure 3. Schematic for experimental setup for voltage clamp experiments. Two glass electrodes were used to penetrate the membrane of either LC 1, 2, or 3. One electrode measures membrane potential, and the other injects current depending on the error signal, where error depends on the desired command voltage.

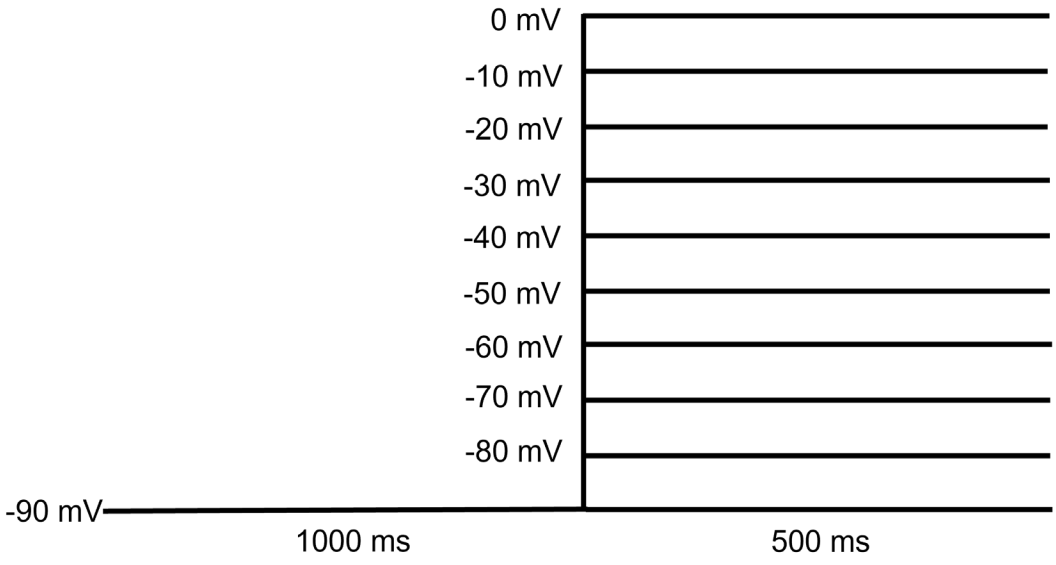

Figure 4. Voltage protocol for investigating total outward current. Holding at -90 mV deinactivates all outward currents, including A-type potassium current, and allows us to measure maximal outward current.

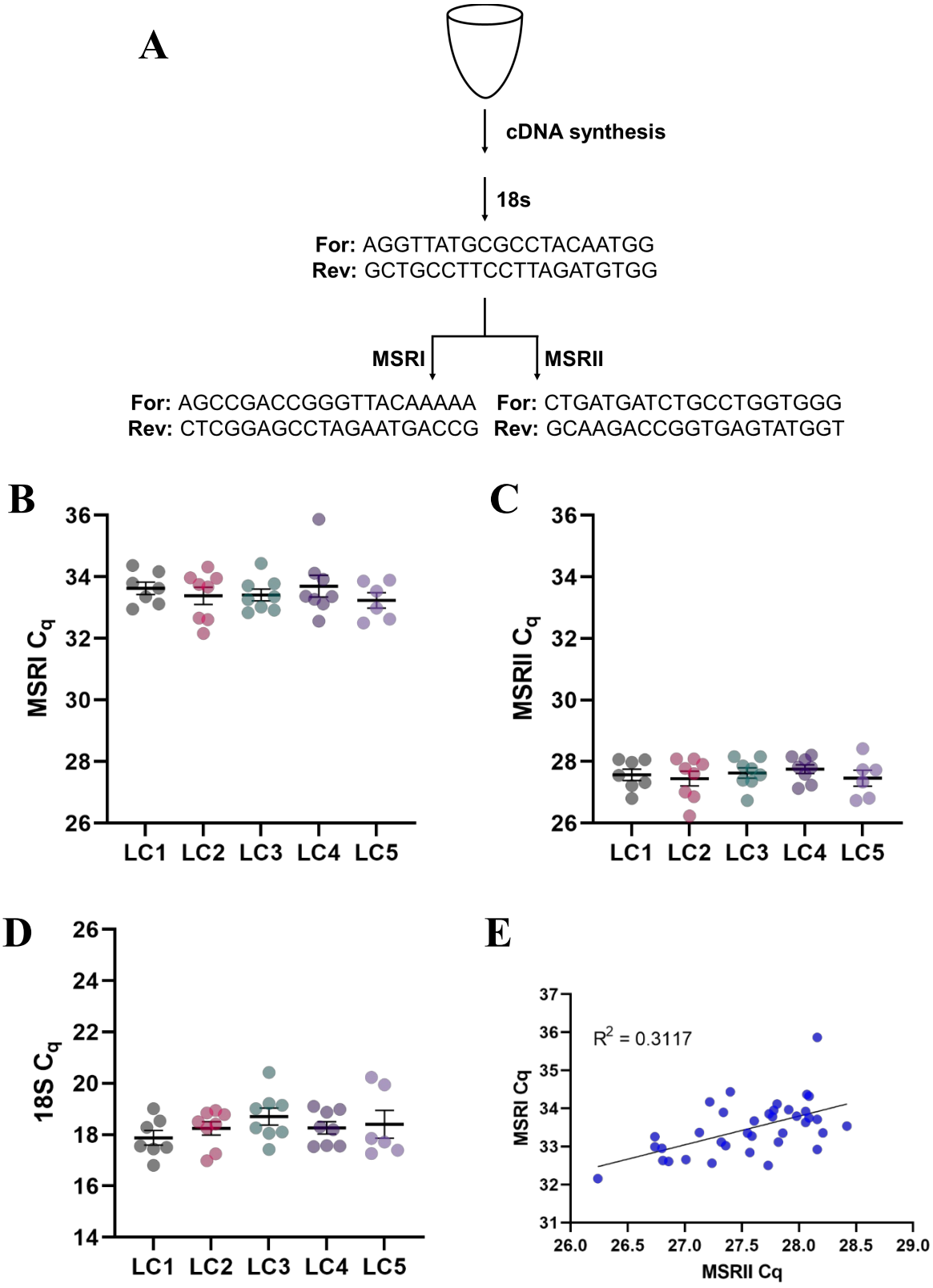

Figure 5. Quantitative single cell RT-PCR analysis of myosuppressin receptor I and II expression in individual motor neurons. (A) Experimental paradigm. Individual large cells were collected, mRNA was extracted, and single

strand cDNA synthesis was performed. qPCR reactions were then performed against 18S rRNA, MSRI, and MSRII mRNA using target-specific primers (pictured). (B, C) MSRI and MSRII expression was the same across motor neuron cell types. MSRII expression was 60-fold higher than MSRI expression. The levels of MSRI expression suggest that it is absent from CG motor neurons. (D) 18s expression was the same across all motor neurons, indicating that individual cells were successfully isolated. (E) MSRI and MSRII mRNA copy numbers are positively correlated, indicating that cells with more mRNA have more of each receptor. There is no evidence of coregulation of MSRI and MSRII in motor neurons.

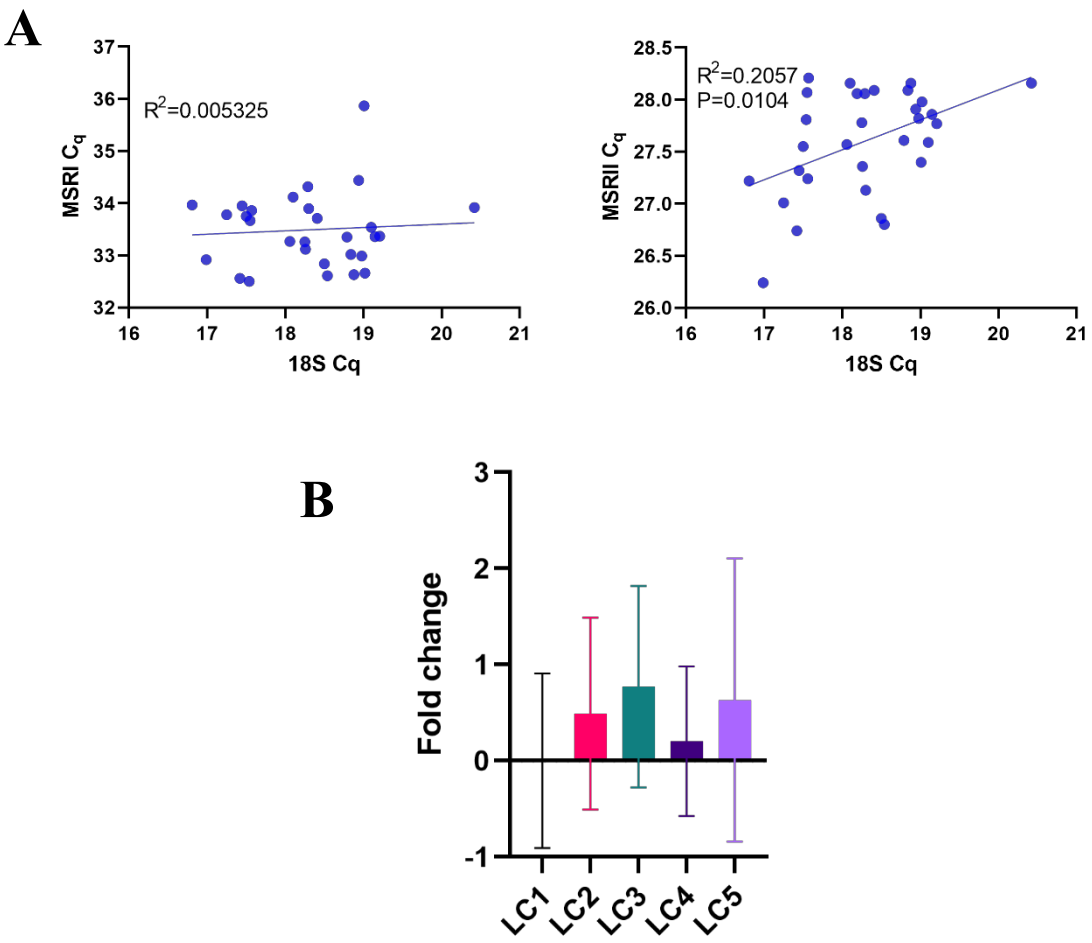

Figure 6. Alternative analysis to quantitative single cell RT-PCR data. (A) To examine if MSR expression was related to the amount of RNA in each sample, we correlated MSRI (left) and MSRII (right) C_q values to 18S rRNA C_q values. MSRI expression levels did not correlate with 18S rRNA levels, but MSRII expression levels did. (B) Using the $2^{-\Delta\Delta Ct}$ method normalizing to 18S as a reference gene and LC1 as an arbitrary control condition, MSRII expression levels did not vary between cell type. Error bars represent range in the fold change in MSRII expression, calculated from the standard deviation for $\Delta\Delta C_q$.

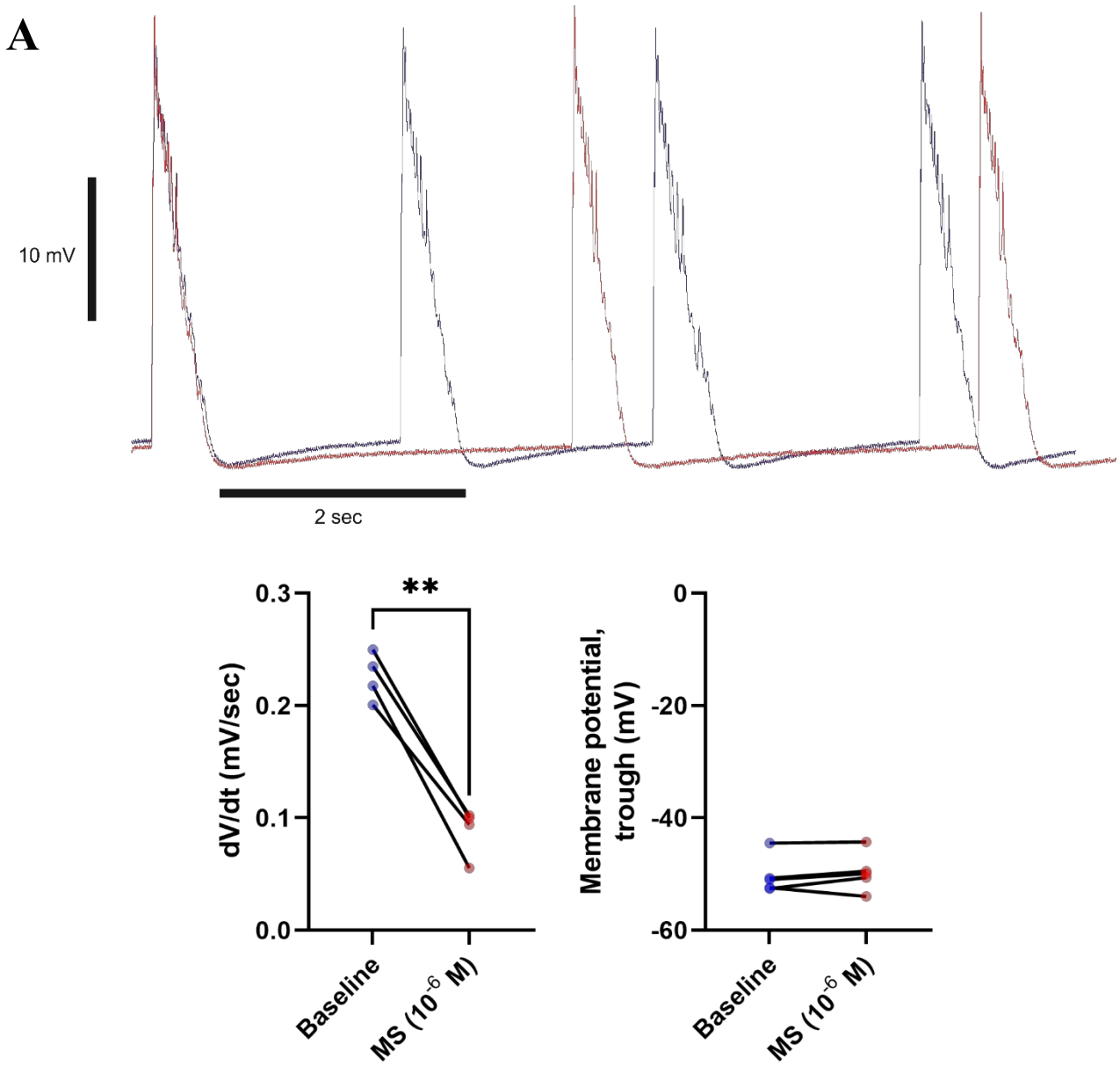

Figure 7. Intracellular recordings of motor neurons in the intact cardiac ganglion in baseline conditions (blue) and myosuppressin (red; 10^{-6} M). (A) The burst frequency of motor neurons decreased substantially, as did the rate of change in the membrane potential during the interburst interval. (B) The rise over run (dV/dt) during the interburst interval significantly decreased significantly (P=0.0143, paired t-test). The minimum of the afterhyperpolarization of the burst did not significantly change, hovering near -50 mV.

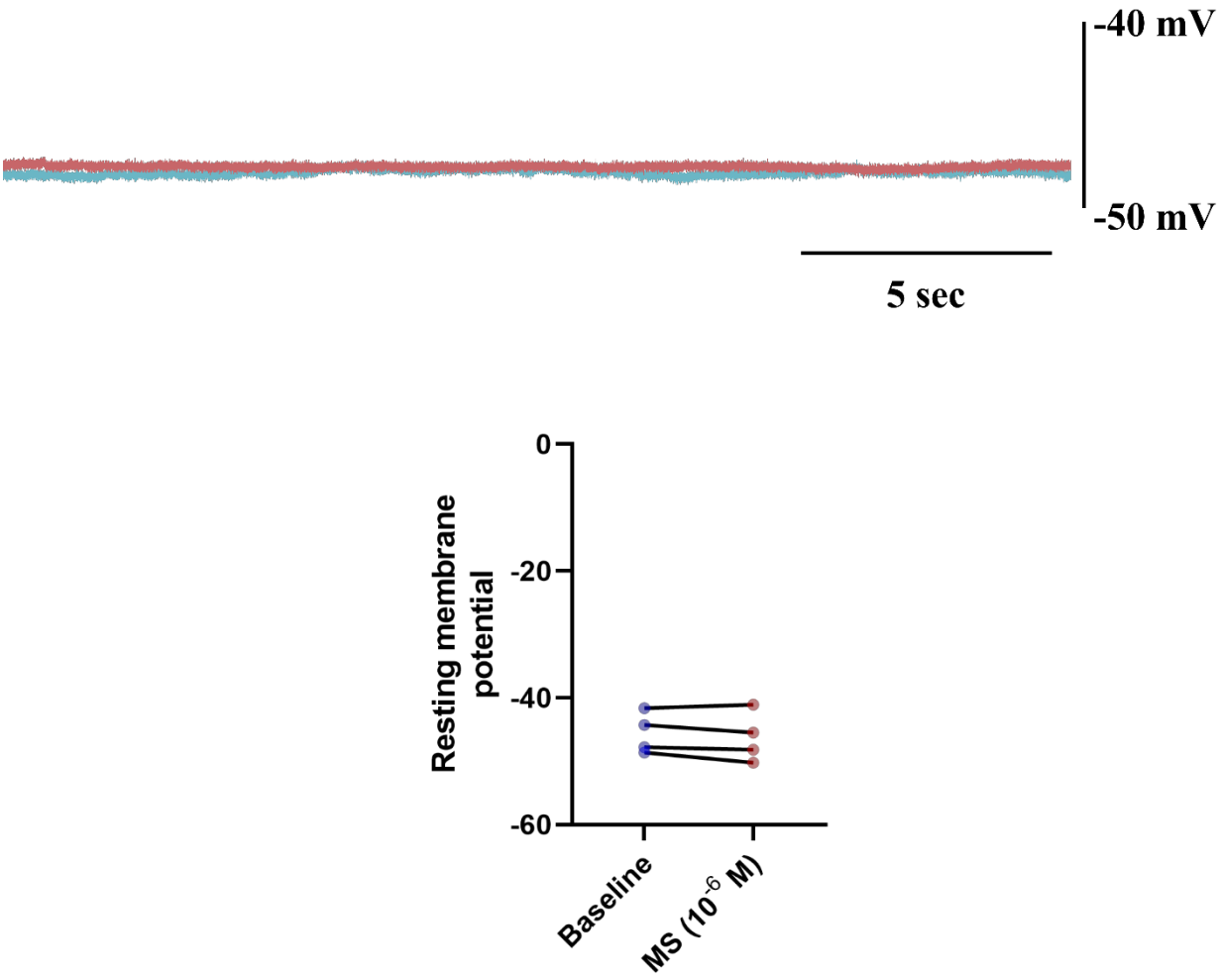

Figure 8. Sharp intracellular recording of cell in saline and TTX (blue) and in TTX and myosuppressin (10^{-6} M) (red). TTX, a fast sodium channel blocker, abolished bursting activity in the cardiac ganglion (top). Myosuppressin failed to change the resting membrane potential after burst activity was abolished (bottom). This indicates that myosuppressin elicits its effects on either a TTX-sensitive channel, or through a current active during rhythmic activity.

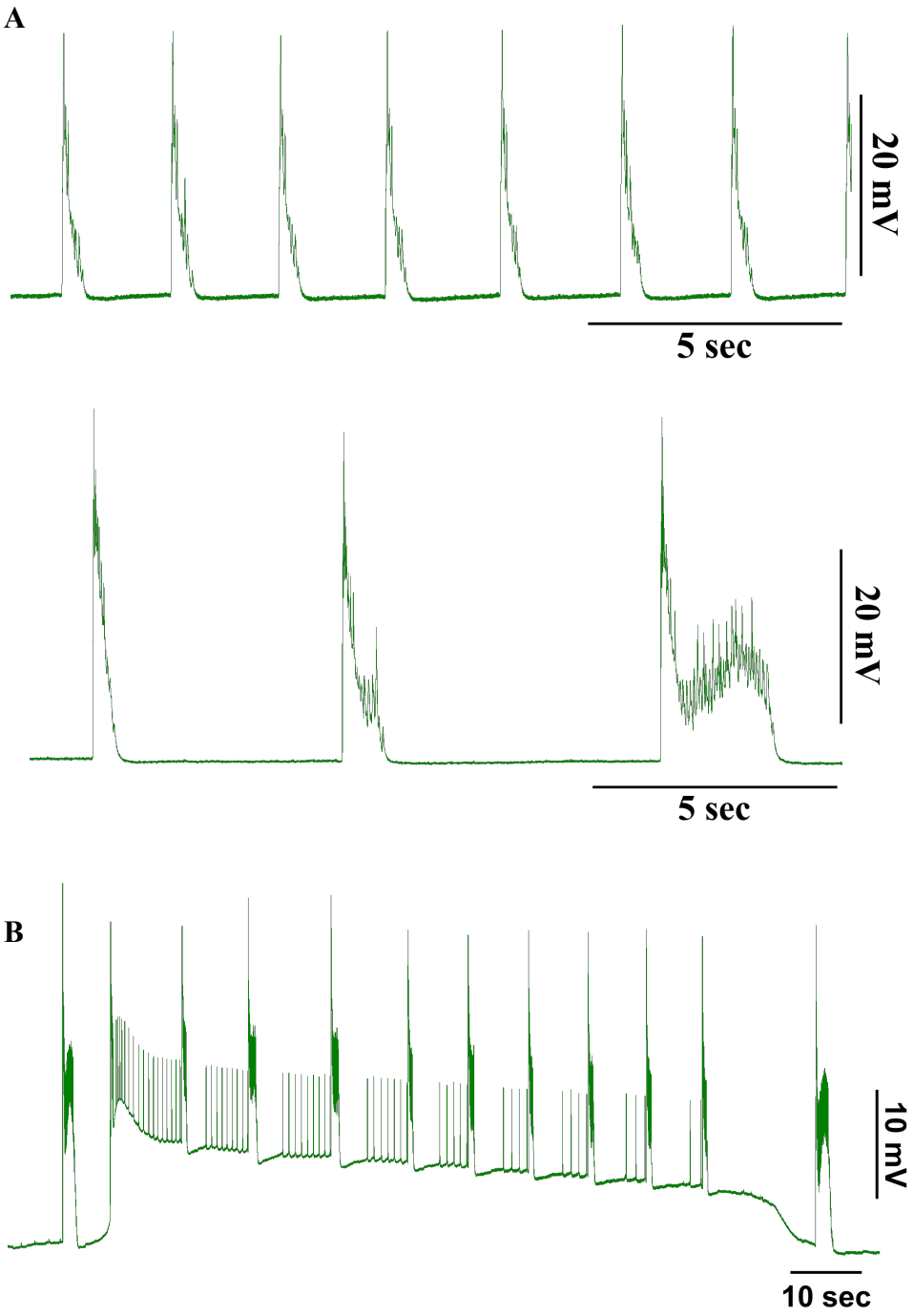

Figure 9. Myosuppressin altered characteristics of individual bursts. (A) Myosuppressin increased burst duration in some cases. Top trace shows a neuron's baseline activity, and the bottom trace shows the neuron's activity during superfusion with myosuppressin. There was variability in duration from burst-to-burst. (B) Prolonged excitation occasionally occurred after treatment with myosuppressin (10^{-6} M). In this neuron, the burst failed to completely terminate, resulting in a prolonged depolarization with tonic firing followed by short bursts of action potentials. This phenomenon happened in this neuron multiple times, indicating that this was not the result of the electrode moving out of the cell.

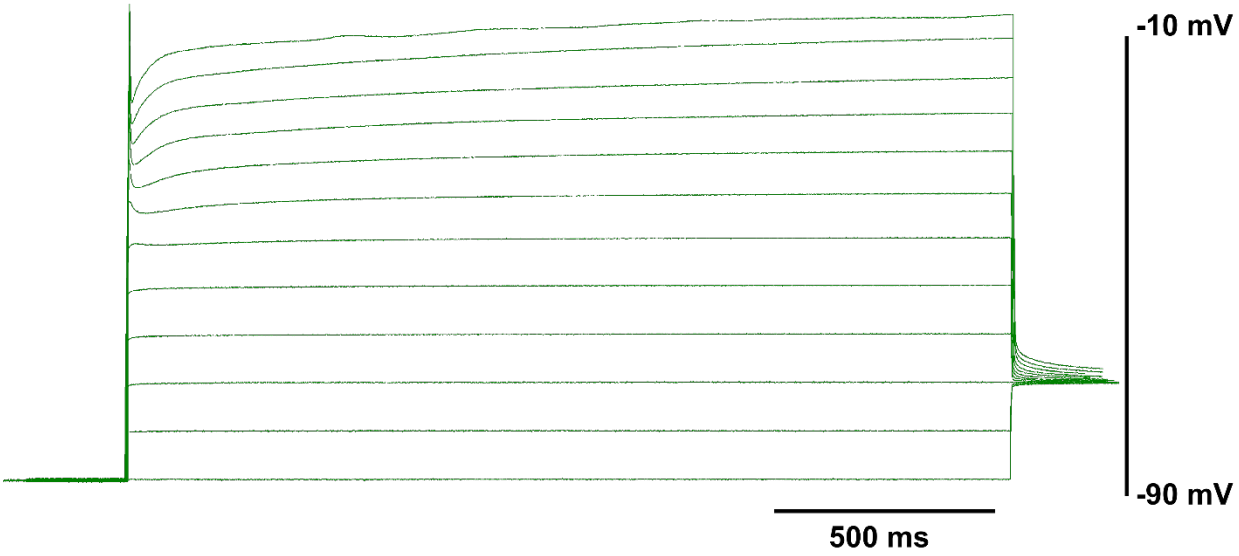

Figure 10. Voltage steps from an actual two-electrode voltage clamp experiments. Note that in this experiment we held the voltage for 2000 ms instead of 500 ms, as indicated in a previous figure. At high voltage steps, the membrane potential did not clamp until after 500 ms.

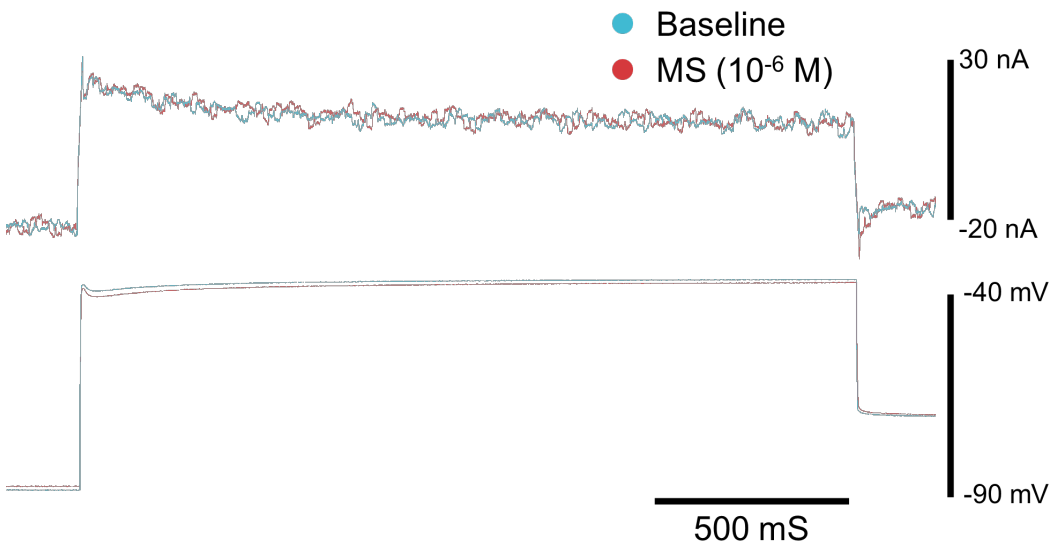

Figure 11. Representative trace of total outward current after a voltage step up to -37 mV. At this step, total outward current occurred in two phases: a transient peak in the first 500 ms followed by a steady state component. Note how neither the peak current amplitude nor the kinetics of current decay differed between baseline (blue) and myosuppressin (red).

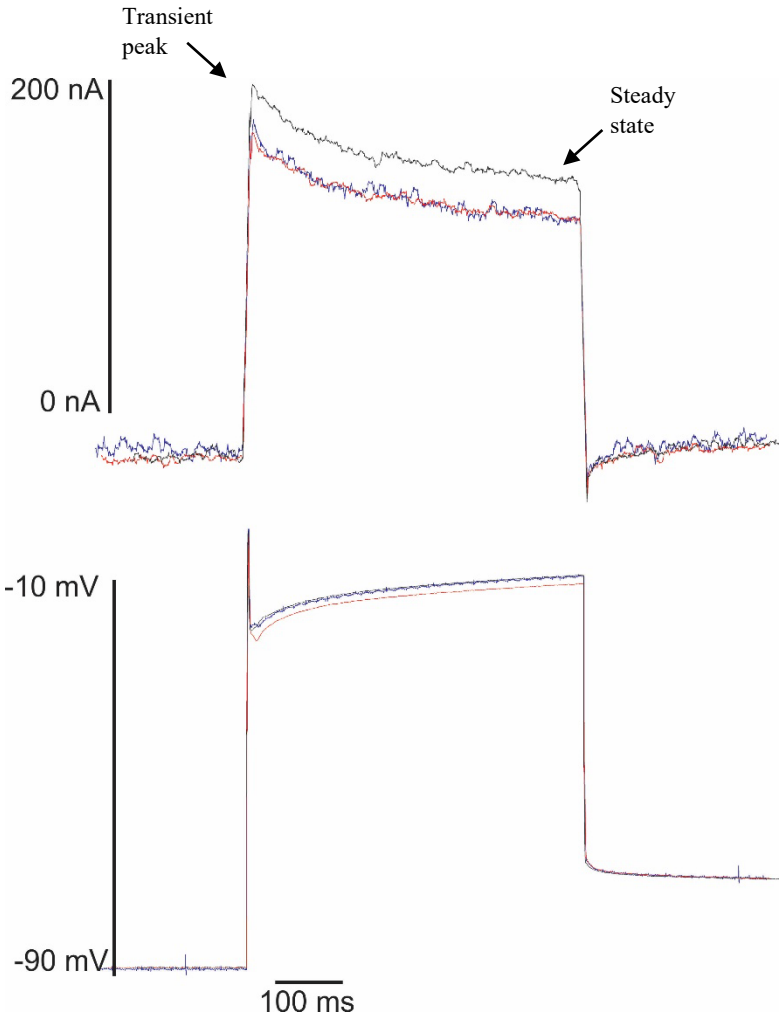

Figure 12. Representative current trace after stepping up to -10 mV in two-electrode voltage clamp. Black=baseline, red=myosuppressin, blue=wash. Note the two main components of the outward current: a transient peak and steady-state component occurring after the peak decays. The current appears to decrease during treatment with myosuppressin, but fails to return to baseline, indicating that the effect was likely an artifact.

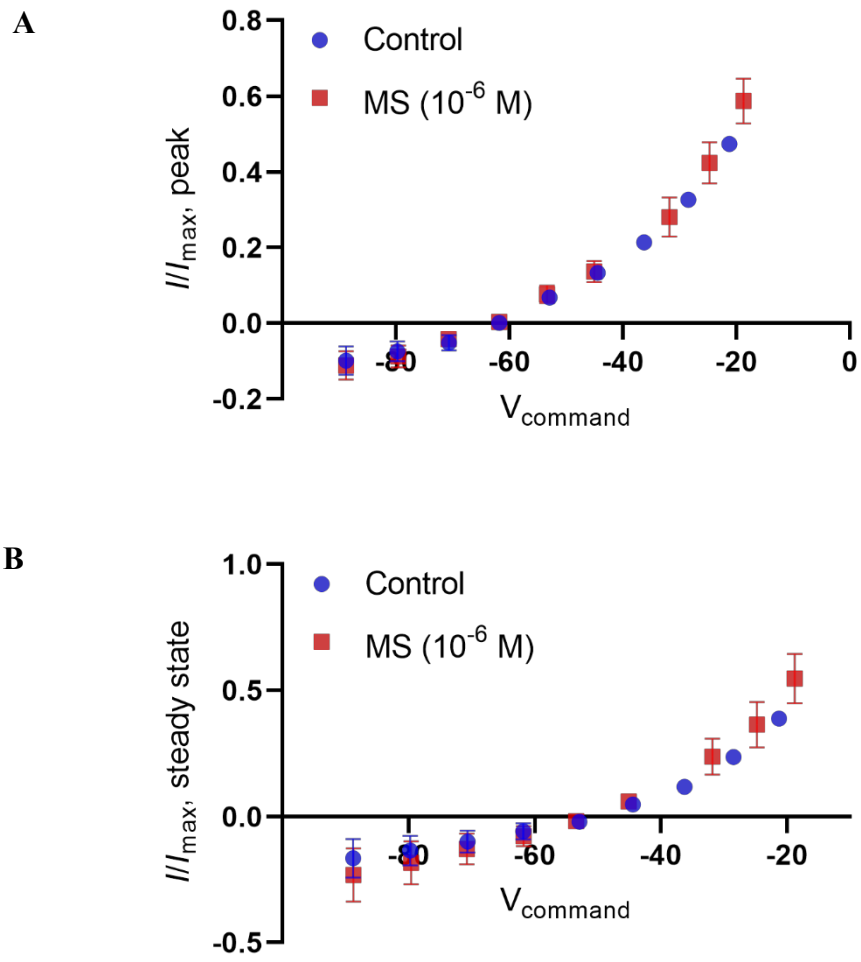

Figure 13. Current-voltage (*I/V*) relationship of total outward current (n=3 cells) in saline (blue) and myosuppressin (red). (A) The *I/V* curve for the peak transient outward current did not change during superfusion with myosuppressin. (B) The steady state outward current did not substantially change during superfusion with myosuppressin. There was, however, a slight increase in the slope, indicating a possible change in the leak conductance according to the equation $I=G(V - E_{reversal})$.

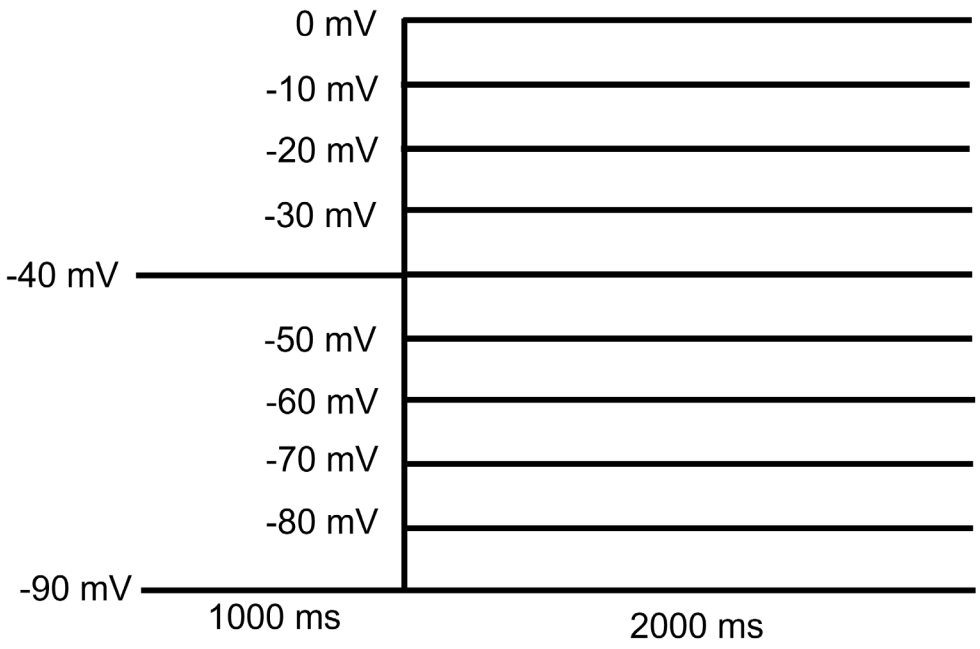

Figure 14. Voltage step protocol for isolating I_A. Membrane potential is held at either -40 mV or -90 mV, then stepped from -90 mV to 0 mV in increments of +10 mV. Holding at -90 mV allows us to obtain total outward current. Holding at -40 mV inactivates I_A, and allows us to obtain all outward current minus I_A. Subtracting current traces thus allows us to isolate I_A.

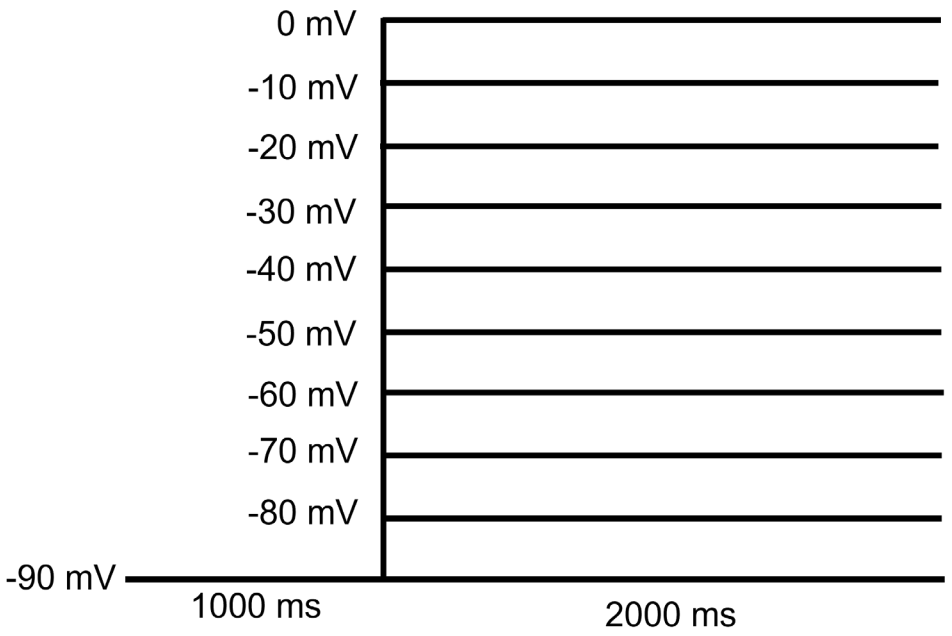

Figure 15. Voltage step protocol for isolating I_{KCa}. The protocol is performed in physiological saline and myosuppressin (10^{-6} M) and then repeated in the presence of Cd^{++}. Cd^{++} ions block calcium channels; thus, in Cd^{++}, all outward currents except I_{KCa} are obtained. This can be subtracted from current recordings in the absence of Cd^{++} to isolate I_{KCa}.